BMC Materials

REVIEW

Open Access

Supercapacitors with alternating current line-filtering performance

Doudou Zhao[1,2], Kaiyue Jiang[2], Jiantong Li[3], Xiang Zhu[4], Changchun Ke[5], Sheng Han[2*], Emmanuel Kymakis[6*] and Xiaodong Zhuang[1,7*]

Abstract

Alternating current (AC) line filters have been widely used to smooth the leftover AC ripples on direct current voltage. Currently available commercial aluminum electrolytic capacitors (AECs) are primarily used for this application. However, the bulky volume and low capacitance of AECs have become incompatible with the rapidly developed intelligent electronic devices and industry dynamics. Supercapacitors with high specific capacitance and AC line-filtering performance could become the next-generation candidates to replace AECs for smoothing leftover AC ripples. Thus, most conventional supercapacitors behave like a resistor and not a capacitor at 120 Hz mainly because complex pore structures of electrode materials prevent the diffusion of electrolyte ions. Various electrode materials have been reported to reveal supercapacitors with AC line-filtering performance; however, the balance of high specific capacitance and an excellent filtering efficiency is a prodigious challenge. This review summarizes recently reported supercapacitors based on different types of electrode materials with AC filtering performance and attempts to develop the relationship between different influencing factors and features of functional materials.

Keywords: Supercapacitor, Micro-supercapacitor, Alternating current line filtering, Phase angle, Electrode

Introduction

Direct current (DC) and alternating current (AC) voltages are used for the conduction and transmission of electrical energy. Compared with DC, AC can be boosted or lowered through transformers [1]. Large-scale electricity applications, such as long-distance transmission, enterprise electricity, and household electricity, generally use AC, whereas some small electronic daily-use devices, such as mobile phones, flashlights, and remote controls, use DC. Some require the conversion of AC into constant DC. To produce constant DC voltage, a rectifier is required to convert AC voltage into unidirectional rectified DC voltage. The rectified DC voltage ripples must be further smoothed using electronic filters to produce stable and constant DC voltage [2]. The AC line filters are used to smooth residual AC ripples generated on DC voltage supply equipment, and to satisfy the current large-scale power demand, the AC filter must be installed in a capacitor with large capacitance. Aluminum electrolytic capacitors (AECs) are widely used as power devices for AC filtering applications [3]. However, the capacitance of AECs is of a lower order of magnitude than that of electrochemical capacitors (ECs); meanwhile, the rigid shape and bulky volume are increasingly incompatible with rapidly miniaturized electronics and flexible systems [4]. Therefore, the development of capacitors with high specific capacitance that can replace AECs with AC

*Correspondence: hansheng654321@sina.com; kymakis@hmu.gr; zhuang@sjtu.edu.cn; zhuang@cczu.edu.cn
[1] The Meso-Entropy Matter Lab, School of Chemistry and Chemical Engineering, Shanghai Key Laboratory of Electrical Insulation and Thermal Aging, State Key Laboratory of Metal Matrix Composites, Shanghai Jiao Tong University, Dongchuan Road 800, Shanghai 200240, China
[2] School of Chemical and Environmental Engineering, Shanghai Institute of Technology, Haiquan Road 100, Shanghai 201418, China
[6] Department of Electrical and Computer Engineering, Hellenic Mediterranean University, Estavromenos, 71410 Heraklion, Crete, Greece
Full list of author information is available at the end of the article

filter performance is essential for the future development trend.

Among various types of electrochemical energy storage devices, supercapacitors have received particular attention of scientific and industry communities in recent years because of excellent superior power density, rapid charge/discharge rate, and outstandingly long lifecycle [5–7]. Supercapacitors can be categorized into two types, namely electrical double-layer capacitors (EDLCs), where charge storage occurs through physical adsorption of ions, and pseudocapacitors (PCs), where the chemical adsorption of ions is attained through redox active materials, such as many metal oxides [8–11]. As energy storage devices, they depend on DC power. Because of a complex microporous structure in a carbon-based electrode, the EDLC-type supercapacitors conventionally exhibit large electrochemical resistance and can be rarely charged and discharged at a frequency higher than 1 Hz [12, 13]. The porous electrodes lead to poor performance for AC line filtering and thus hinder the elimination of residual AC ripple from rectified current [14]. For PCs, because of inherently low charge transfer on the electrolyte/electrode surface of the electrode material [15], capacitors behave like resistors and not capacitors in 120 Hz, which impedes their applications in AC line filtering [4, 16–18].

The unsatisfactory frequency response of supercapacitors is primarily attributed to the large series resistance of electrode materials and complex microporous structures. In 2010, Miller and coworkers reported that vertically oriented graphene nanosheet (VOGN) electrodes prepared through chemical vapor deposition (CVD) show excellent AC filtering performance [16]. It became the beginning of a new generation of capacitors with AC filtering performance, which then inspired numerous researchers to develop electrode materials with AC filtering performance, such as various types of graphene, electrochemically reduced graphene oxides (ErGOs), ordered mesoporous carbon (OMC), carbon derivatives, conducting polymers, and metal oxides [1–28]. This review aims to summarize the recently developed supercapacitors based on different types of new materials with AC filtering performance and attempts to understand the relationship between these materials and AC line-filtering performance.

To promote the application of supercapacitors in the AC line-filtering frequency response, the reported supercapacitors were classified based on electrode materials. It is hoped that classification can provide convenience for the development of new materials for AC filtering. "Key factors of an AC line filter" section presents the main factors of the AC line filter. The carbon-based electrode materials, conductive polymer-based electrode materials, and transition metal-based nanomaterials are summarized in "Carbon-based electrodes", "Conducting polymer-based electrodes" and "Transition metal-based electrodes" sections. The prospect and summary of supercapacitors with AC filtering performance are illustrated in the final section.

Key factors of an AC line filter

Figure 1a shows the full-wave bridge alternating current through AC line filtering to convert AC power into DC power. First, the AC input signal comprises a function generator. Second, a full-bridge square array comprising four diodes converts AC input signals into pulsating DC signals. Finally, the supercapacitor converts the rectangular pulse signal into a smooth DC output. The fundamental principle of frequency response is examined, and the review provides the primary reference guide for the future research and design of supercapacitors with AC filtering performance. Electrochemical impedance spectroscopy is one of the main methods to study capacitors with AC filter performance, wherein a low frequency response represents capacitance characteristics [29, 30]. The overall impedance models of PCs and double-layer capacitors (DLCs) are similar, although they show different behaviors because of different frequency ranges [31, 32]. The curve of the impedance phase angle with frequency illustrates the performance gap in terms of frequency response between the conventional EC and commercial AEC (Fig. 1b). Figure 1c shows the general capacitor impedance behavior, including three major regions, namely a high-frequency semicircle, an intermediate frequency Warburg impedance, and a low-frequency capacitance behavior. The semicircle represents the charge transfer resistance formed at the interface between the electrode and electrolyte at the beginning of the electrochemical reaction [33]. The medium-frequency region represents the characteristic of the rapid diffusion of ions to the electrode, and the high-frequency region represents the impedance of charge transfer associated with the Faraday redox reaction of the electrode material [34]. Figure 1d describes the relationship between the phase angle of impedance and frequency, which is termed the Bode phase diagram. The impedance diffusion behavior of the electrode material corresponds with the Bode diagram on the right [35, 36]. A gradual transition is observed from the second region to the third region in the impedance spectrum, which corresponds to the gradual increase in the phase angle in the Bode diagram to reach a near optimally stable value of approximately 90° [37]. The phase angle at 120 Hz was the primary indicator for measuring AC line-filtering performance.

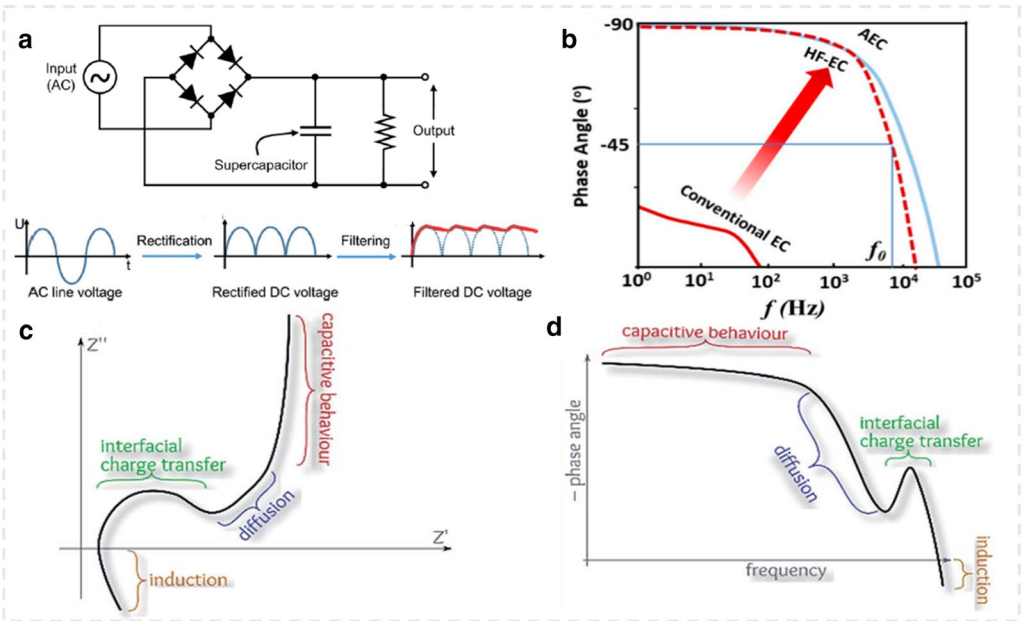

Fig. 1 **a** Electrical circuit diagram of AC line filtering and the conversion of AC line voltage into DC voltage; **b** plot of an impedance phase angle versus the frequency illustrates the performance gap in terms of frequency response between the conventional EC and AEC; **c** Nyquist; and **d** Bode plots for a schematic impedance model. Reproduced with permission from Ref [32]. Copyright 2018. The Royal Society of Chemistry

The resistance capacitance (RC) time constant (τ_{RC}) produced using the complete resistance measured under 120 Hz, which was the result of charge (electrons and ions) mobility limitation. The time constant was obtained using the equation ($\tau_{RC} = C \times Z'$), where Z' is the resistance derived from the real part of the impedance, and C is the specific capacitance calculated from the equation $C = -1/(2\pi f Z'')$, with f and Z'' representing frequency (Hz) and imaginary part of impedance (Ω), respectively [38]. The RC time constant of conventional supercapacitors is generally 1 s, which is excessively high for 120-Hz AC filtering with a time period of 8.3 s [39]. Such a high time constant can be attributed to the complex pore structure of supercapacitor electrode materials, which hinders the high-speed diffusion of ions and increases the effective charge transfer resistance [40, 41]. Therefore, to fabricate supercapacitors that meet the performance of AC filtering, electrode materials with a high specific surface area, high conductivity, and highly ordered pore structure, must be designed. Another crucial parameter to detect the performance of AC filtering is the relaxation time constant ($\tau_0 = 1/f_o$), which is the minimum time required to discharge all energy from the device with an efficiency of more than 50% [42]. Characteristic frequency f_0 is the value at a phase angle of 45°. Lower τ_0 corresponds to the prominent rate performance of the supercapacitor, and the ability to maintain capacitive behavior at a high frequency is also reflected when the phase angle is close to the optimal value of 90° [11]. In the design of supercapacitors with AC filtering performance, the ultrahigh rate performance of electrode materials is a necessary characteristic to eliminate high-order harmonics to protect electronic devices from damage [43]. In summary, three primary factors for the preparation of supercapacitor electrode materials with AC filtering properties are as follows: (1) high specific surface area, (2) high electrical conductivity, and (3) ordered pore structure distribution.

Carbon-based electrodes

Carbon-based materials including activated carbon [44], onion-like carbon [41], carbon derivatives carbon [45, 46], carbon nanotubes (CNTs) [17, 30, 47–50], and graphene [51–53] have been intensively applied as electrode materials for supercapacitors. Typical supercapacitors based on these porous carbon electrode materials show a low frequency response and a phase angle of approximately 0° at 120 Hz, which is considerably lower than the optimal 90° for AC line filtering [54]. The main reason is the complex and disordered porous structure of electrode materials, which hinders the transfer of electrons and mass [13]. Therefore, various new carbon-based electrode materials have been developed for a high-frequency response to satisfy the requirements for AC line filtering.

Graphene-based electrode

Graphene-based electrodes have led to extensive research on the application of supercapacitors in recent years because of its inherent high specific surface area and high conductivity. A large number of research results have shown that graphene has great potential in energy storage. Graphene can be used in devices such as micro-capacitors, transparent batteries, and rapid charge–discharge electronic equipment [55–60]. In 2010, for the first time, Miller reported that a VOGN electrode-based capacitor grown on metal current collectors through CVD can be used for AC line filtering [12]. The as-produced capacitor had an RC time constant of 1 s. Figure 2a shows a plain view of a VOGN electrode-based capacitor. The irregular surface is caused by the defect due to external stress and incorporation of hydrogen. Figure 2b shows the impedance phase angle versus the frequency of the VOGN electrode-based capacitor, activated carbon electrode-based capacitor, and commercial aluminum electrolytic capacitor. At 120 Hz, the phase angle of the capacitor based on the graphene nanosheet was 83°, which was close to the phase angle 85° of the AEC, whereas the impedance phase angle of the capacitor based on activated carbon was almost 0°. This difference was almost entirely caused by the complex pore structure of activated carbon. The frequency-dependent capacitance of the graphene nanosheet capacitor shows that the capacitance value was 175 μF and the RC time constant was less than 200 ms at 120 Hz (Fig. 2c). Moreover, some graphene-based electrode materials prepared using the CVD method have been used to increase the frequency of the corresponding supercapacitors [20, 24, 61].

Sheng [9] reported a similar frequency response based on a three-dimensional graphene electrode prepared by the electrochemical reduction of graphene oxide. The as-prepared ErGO electrode comprised a porous 3D interpenetrating layer with a thickness of approximately 20 mm (Fig. 2d). At 120 Hz, the phase angle of ErGO-DLC (− 84°) was comparable to that of commercial aluminum electrolytes (− 85.5°) at 120 Hz (Fig. 2e). The maximum area capacitance of the capacitor was 325 μF cm^{-2} at the lowest frequency of 1 Hz (Fig. 2f). However,

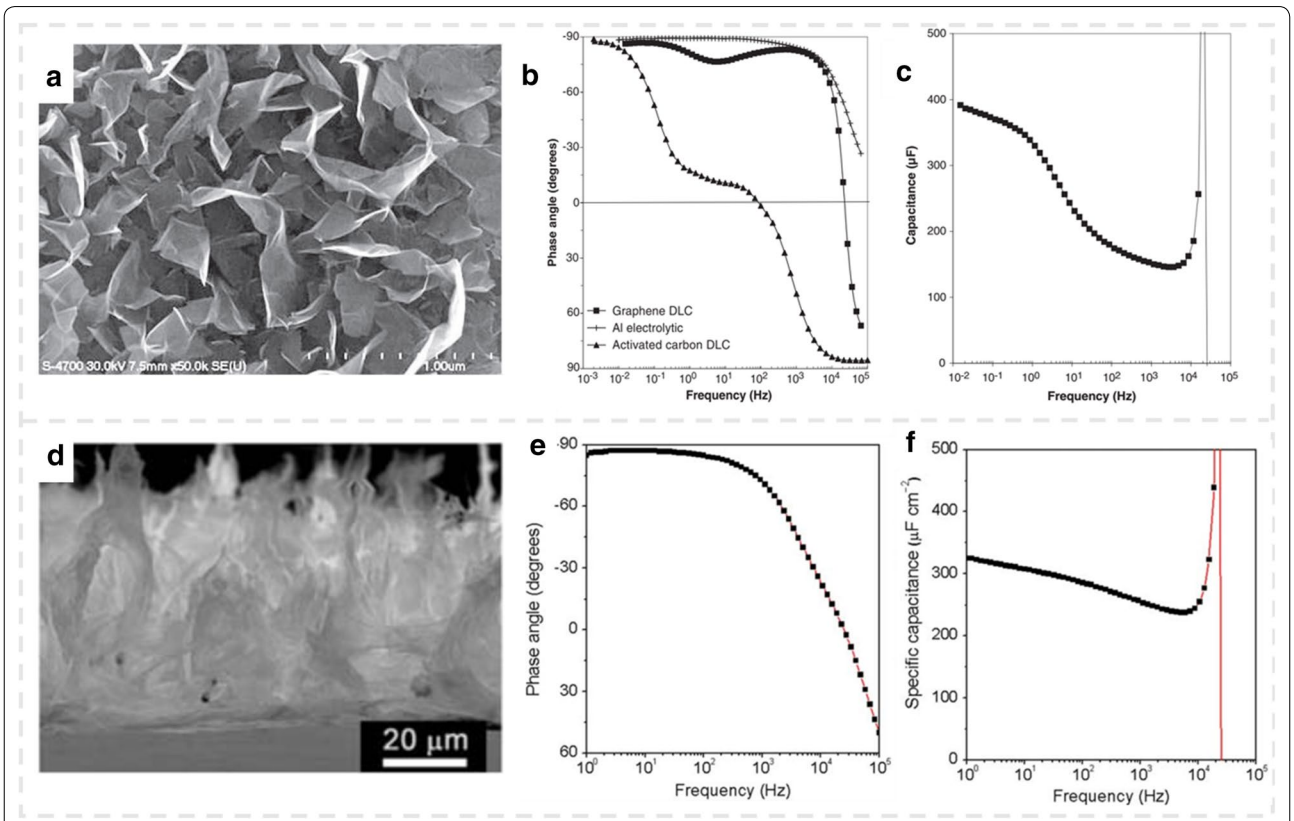

Fig. 2 **a** Scanning electron microscope (SEM) micrograph vertical aligned graphene on the Ni surface; **b** impedance phase angle versus the frequency for a graphene nanosheet-based capacitor, commercial aluminum electrolytic capacitor, and activated carbon-based capacitor; **c** capacitance versus the frequency of the graphene nanosheet capacitor; Reproduced with permission from Ref [12]. Copyright 2019. AAAS. **d** cross-sectional SEM image of the ErGO electrode; **e** plot of the impedance phase angle versus the frequency; and **f** plot of specific capacitance versus the frequency. Reproduced with permission from Ref [9]. Copyright 2012. Macmillan Publishers Limited

the excellent frequency response caused by low specific capacitance at the cost of a low material density load could not satisfy practical requirements. The primary reason is that supercapacitors with graphene-based materials as electrode materials are frequently affected by the accumulation of graphene sheets during processing. In response to the aforementioned problems, Yoo and coworkers [62] fabricated in-plane and ultrathin supercapacitors, wherein the surface of each layer of graphene could be used to store energy. Compared with the conventional two-dimensional stacked electrode, the planar design resulted in a dramatic increase in capacitance.

On the basis of the design of this type of planar electrodes, with the rapid development of miniaturized electronic equipment, the demand for compact energy storage on-chip is increasing day by day. Compared with conventional AECs, the in-plane micro-supercapacitors (MSCs) have higher volume energy density and a more compact structure. Therefore, the development of planar MSCs with an AC line-filtering function is an ideal alternative to replace AECs and integrate with other electronic units. Kaner and coworkers [63] reported the scalable fabrication of graphene MSCs, which could be developed on a large scale by using a standard LightScribe DVD recorder for direct laser writing on graphite oxide films. The laser-scribed graphene (LSG)-based MSCs exhibited a suitable frequency response in a short relaxation time (Fig. 3) compared with commercial AC supercapacitors and AECs. Figure 3a–c show the preparation process of the photolithographic graphene electrode and the assembly of the device. Figure 3b shows the morphology of the film after the laser treatment. The film expanded, and thus, the film could be in complete contact with the electrolyte, which was essential for the

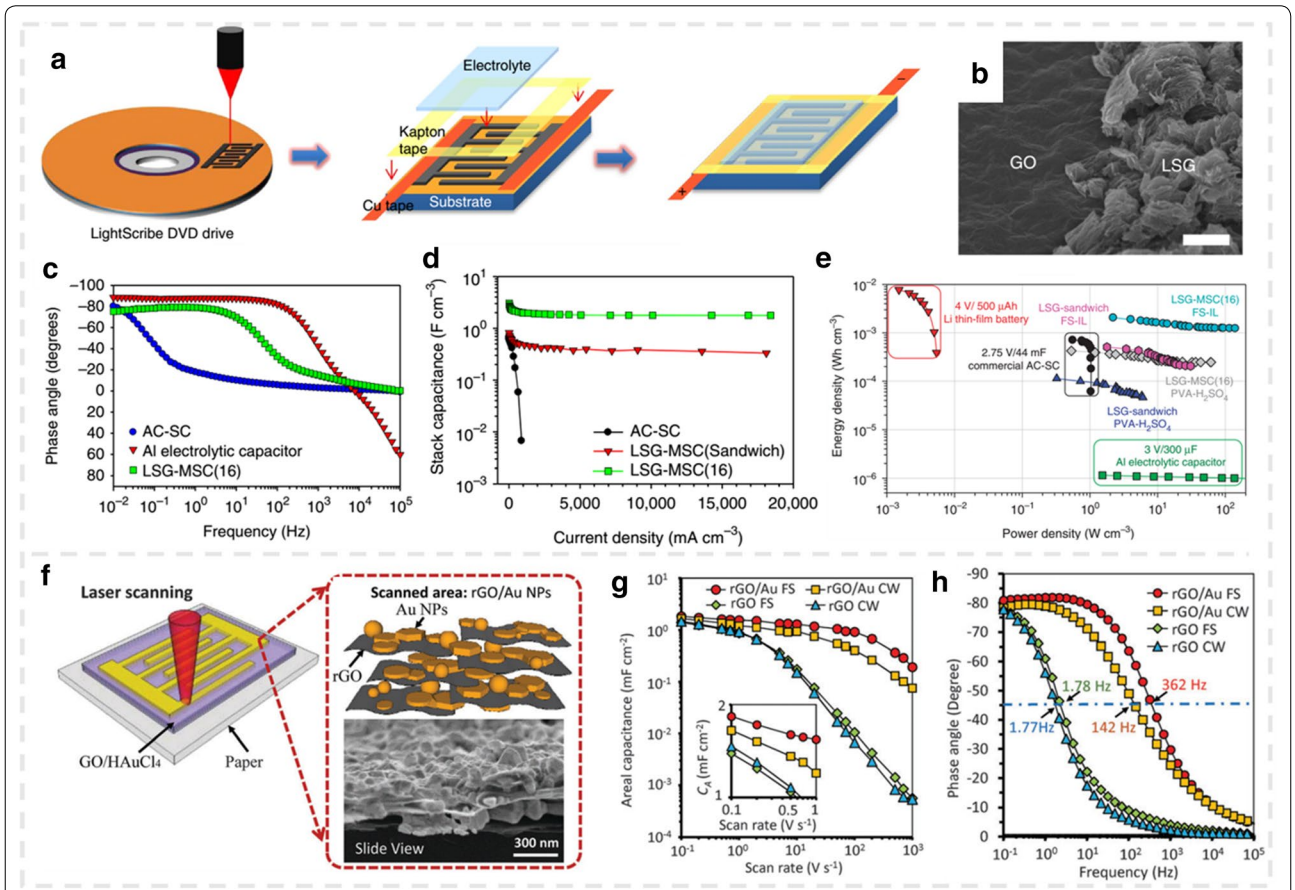

Fig. 3 **a** Schematic of the fabrication process for an laser scrbed graphene (LSG) micro-supercapacitor; **b** a tilted-view (45°) SEM image shows the direct reduction and expansion of the GO film after exposure to the laser beam, scale bar (10 mm); **c** the impedance phase angle versus the frequency for LSG-MSC compared with a commercial AC-supercapacitor and aluminium electrolytic capacitors; **d** volumetric capacitance of an LSG-MSC and a commercial AC-supercapacitor; **e** Ragone plots of LSG-MSCs compared with commercially available energy-storage systems; Reproduced with permission from Ref [63]. Copyright 2013. Macmillan Publishers Limited. **f** Direct femtosecond laser writing of rGO/Au microelectrodes; **g** areal capacitance as a function of the scan rate (inset shows a magnified low-scan-rate region); and **h** Bode plot of impedance of the rGO-based MSCs. Reproduced with permission from Ref [64]. Copyright 2016. Macmillan Publishers Limited

charge–discharge performance of the electrode. Furthermore, such LSG-MSCs have an extremely small relaxation time (Fig. 3c), thus showing an excellent frequency response. Figure 3d shows the volume capacitances of the LSG-MSC, AC supercapacitors, and AECs. At a current density of 16.8 mA.cm^3, the stack capacitance of LSG-MSC was 3.05 F cm^{-3}, which was approximately three orders of magnitude higher than the conventional discharge current density used to evaluate conventional supercapacitors. The LSG microdevice showed three times higher energy density and 200 times higher power density compared with the Ragone plots of carbon-based supercapacitors (Fig. 3e).

The LSG-MSC has a power density equivalent to AECs and provides an energy density of more than three orders of magnitude. Figure 3f shows that the femtolaser (FS) reduced the $HAuCl_4$ coating on Au nanoparticles and inserted it into an RGO to form a stacked structure for a RGO-Au microelectrode, which significantly improved the conductivity of the electrode reported by Hu and coworkers [64]. The area capacitance of RGO-Au FS-MSCs was evidently higher than that of other electrodes prepared using the FS method at the same scanning speed (Fig. 3g). This advantage was more evident at high scanning rates. Furthermore, the as-fabricated rGO/Au FS-MSCs satisfied the requirement of AC line filtering in the high-frequency region. The as-produced RC time constant was 2.76 ms when the characteristic frequency at the phase angle was 45° (Fig. 3h). The RGO/Au electrode obtained using the FS etching increased the conductivity of the electrode by two orders of magnitude to 1.1×10^6S m^{-1}, and the planar inter-digital electrode shortened the ion diffusion distance. The fabricated supercapacitor has a high-frequency response, large specific capacitance (0.77 mF cm^{-2} at 1 V s^{-1}), and outstanding cycle stability. These improvements in the electrode design are expected to lead to an ideal energy density for supercapacitors.

Nitrogen doping for graphene was reported to significantly improve the specific surface area and electrical conductivity of electrode materials, which were the most crucial features of energy storage materials. The radius of N is close to C, making N easy to replace carbon atoms in the atomic lattice, and further resulting in the formation of N-doped carbon materials. The nitrogen atom has one more extra-nuclear electron than the carbon atom and has a high electron affinity. Therefore, C atom adjacent to N in the nitrogen-doped carbon material has high positive charge density. At the same time, there is a conjugation channel between N lone pair electrons and large π-bonds in carbon lattice, rendering N-doped carbon materials with excellent electrochemical properties. [65, 66] As a conventional application, the research on ultrahigh power DLCs for AC line filtering was presented. Kim and coworkers [67] proposed a controllable method to customize the complete crystalline graphene nanostructure through the specific decompression of CNT heteroatom dopants. The cooperative nanostructure exhibited a large specific surface area and strong electrical connectivity and showed the performance of ultrahigh power supercapacitors, which could be used for AC line filtering with a record high-speed capability of a phase angle of 85° at 120 Hz. Figure 4a shows the electrochemical decompression process of a nitrogen-doped CNT (NCNT) forest in 1 M H_2SO_4 at a potential of 0.6–0.8 V. The SEM image validated that the carbon nanostructure comprising unzipped graphene nanoribbons wrapped around the NCNT core (Fig. 4b). The atomic-force microscopy (AFM) image showed that the 1.7-nm-thick three-layered graphene sheets were produced from 5.9-nm-diameter triple-walled NCNTs (Fig. 4c). The impedance phase angle spectrum further validated that the unzipped structure exhibited excellent AC filtering performance. Figure 4d compares the impedance phase angles of DLCs at different frequencies of unzipped, original NCNT forests and conventional AECs at different frequencies. Moreover, a 1-mm-high unzipped nanostructure of DLCs could reach up to a phase angle of 45° at 8.1 kHz and exhibited the impedance phase angle of 85°, which was comparable to that of the AEC or other reported DLCs. Figure 4e presents the specific capacitance and RC time constant. Moreover, a 5-mm-unzipped structure-based DLC exhibited 402 mF cm^{-2} at 120 Hz, which was considerably higher than 230 mF cm^{-2} of the 5-mm-NCNT-DLC (Fig. 4f). Furthermore, the RC time constants of DLCs fabricated using a 5-mm-NCNT forest, 5- mm-unzipped structures, and 1-mm-unzipped structures were 616, 468, and 212 μs at 120 Hz, respectively. These values were adequately smaller than the standard period of 8.3 ms, which was crucial for effective AC line filtering at 120 Hz. The unzipped nanostructures showed a small relaxation time constant ($\tau_0 = 0.25$ ms) at 1 mm, which indicated that DLCs constructed with the customized unzipped structures have not only ultrahigh power performance but also a large specific capacitance at 120 Hz. Although heteroatom doping could increase the conductivity of the material to a certain extent, through some research attempts, heteroatom doping is not suitable for eliminating AC filtering. This could be the induction of active scattering centers by heteroatoms in the carbon lattice, and therefore the electrons dispersing and the discharge rate of the charge are both hindered [66].

To satisfy the growing demand for portable, wearable, and implantable electronic devices, high-performance and flexible MSCs have a prominent application

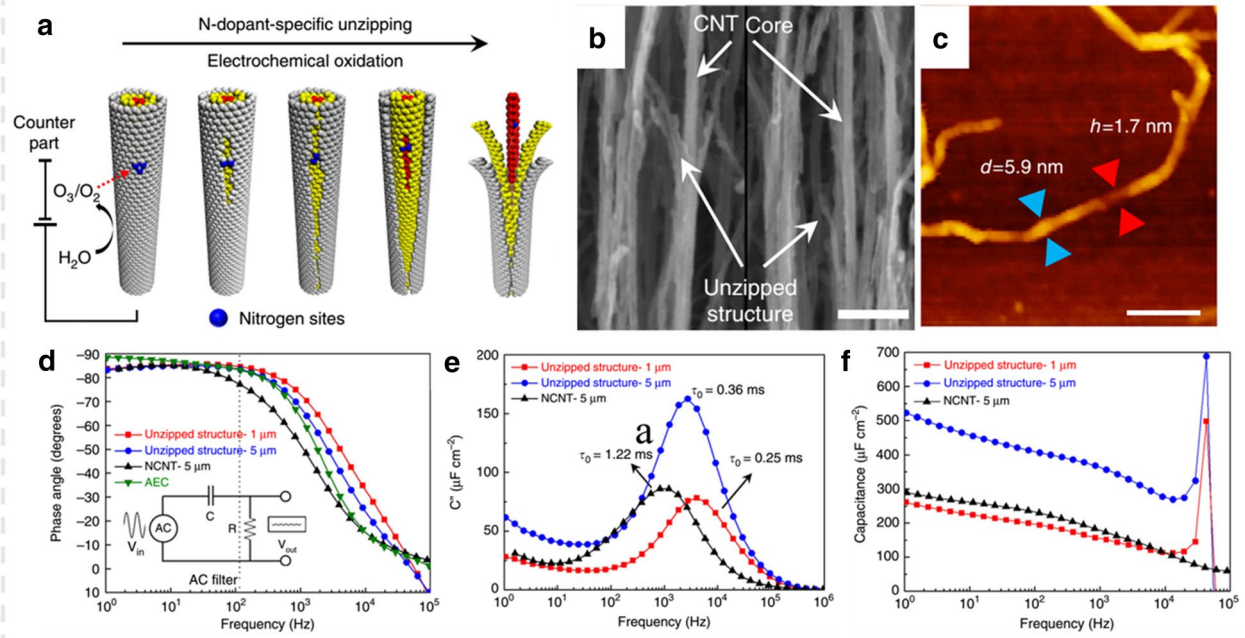

Fig. 4 **a** Schematic of the N-dopant specifically unzipping of NCNTs; **b** SEM image of the unzipped nanostructure; **c** AFM image of the unzipped nanostructure; blue and red arrows indicate NCNT and graphene nanoribbons, respectively; **d** AC impedance phase angle versus the frequency (vertical dotted line indicates 120-Hz frequency); **e** imaginary part (C″) of specific capacitance versus the frequency; and **f** specific capacitance versus the frequency assuming a series RC circuit model. Reproduced with permission from Ref [67]. Copyright 2016. Macmillan Publishers Limited

prospect. Direct laser writing (DLW) technology provided a favorable protocol for the fabrication of flexible, high-performance miniature supercapacitors that satisfied the requirements. Zhu and coworkers [68] developed graphene-based MSCs (MG-MSCs) through the DLW of stacked graphene films made through industry-scale CVD. Figure 5a shows the fabrication process of flexible all-solid-state MG-MSCs. Furthermore, the MG-MSCs demonstrated an outstanding AC line-filtering performance, which indicated the phase angle of 76.2° and a RC constant of 0.54 ms at 120 Hz. Figure 5b compares the parameters of AC filter performance with those of the reported supercapacitors, which further illustrated the application prospects of MG-MSCs in a flexible AC line changer.

The Ragone graph, which compared the power density and energy density performance of MG-MSCs with those of different types of MSCs is presented in Fig. 5c. The MG-MSCs exhibited an exceptional energy density of 23 mWh cm^{-3} at 0.32 W cm^{-3} in an ion-gel electrolyte, which was higher than those of other carbon-based thin-film MSCs, such as doped graphene (sulfur-doped graphene, SG-MSCs, 12.4 mWh cm^{-3}; nitrogen and boron codoped graphene, BNG-MSCs, 16.9 mWh cm^{-3}) [69], MPG-MSCs (7.5 mWh cm^{-3}) [70], photochemical reduction of GO/TiO2 composite (PRG-MSCs, ≈13.2 mWh cm^{-3}) [71], and ultrathin printable MSCs (G/PH1000, UPSCs-25, 12 mWh cm^{-3}) [9]. After the function generator inputs the AC signal, the AC signal can be converted into the pulse DC signal by full-bridge rectifier, and finally, the DC output is smoothed by the miniature supercapacitor prepared in the experiment.

CNT-based electrode

Another effective strategy to improve the capacitance of supercapacitors was to add spacers, such as CNTs between graphene sheets to prevent their restacking. Thus, Wang and coworkers [50] developed ultrahigh power density MSCs based on reduced graphene oxide (rGO) and CNT composite electrodes. Figure 6a illustrates the process of fabricating an MSC by integrating electrode materials into a digital inter-Ti/Au microelectrode. Figure 6b shows the SEM image of the rGO-CNT hybrid electrode, which evidently revealed the uniformly filled thin film with the appearance of CNTs between the rGO sheets through the controllable range of deposition, and no evident stacking phenomenon was observed.

As shown in Fig. 6c and d, the specific capacitance increased compared with that of the reported capacitor; however, frequency response performance was poor, which could not satisfy the requirements of AC filtering. Hata and coworkers [48] fabricated MSCs

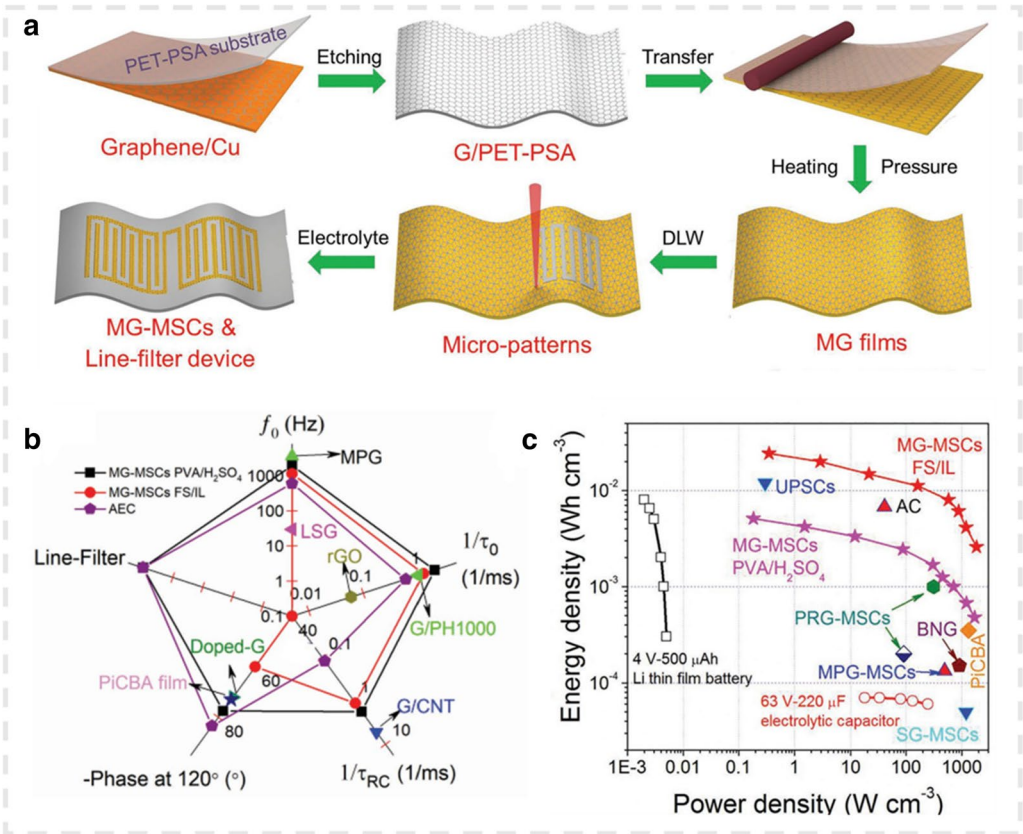

Fig. 5 **a** Schematic of the fabrication process of solid-state flexible MG-MSCs; **b** radar plot of MG-MSCs compared with the AEC and carbon-based MSCs; **c** Ragone plots of MG-MSCs compared with commercial LTF batteries, electrolytic capacitors, and a few developed MSCs. Reproduced with permission from Ref [68]. Copyright 2015. WILEY–VCH

based on the interdigital single-walled CNT (SWCNT) electrode, which solved the large volume problem of AECs in microdevices. The fabrication process of the IEDC is presented in Fig. 6e. From Fig. 6f and g, it can be concluded that the power density of IEDC (2271 W cm^{-3}) was two orders of magnitude higher than that of commercial capacitors (14 W cm^{-3}) and one order of magnitude higher than that of commercial AECs (300 W cm^{-3}). The resulting relaxation time constant (7 ms) could be used in AC filtering for AC–DC conversion.

Flexible and wearable portable electronic devices were inevitably developed to meet increasing social requirements. Flexible microdevices with AC filtering performance were also fabricated to meet these requirements. Xie and coworkers [72] reported an in-plane MSC with AC line-filtering performance based on the SWCNT film and TiO_2 NPs. Figure 7a shows the fabrication process of the microdevice. The SWCNT enhanced the stretchability of SWCNT microelectrodes. Figures 7b and c compared the optical photographs of the microdevices at a telescopic pressure of 200 and without any pressure, respectively. Figure 7e presents the phase angles under different telescopic pressures.

At present, flexible supercapacitors with AC filtering performance are limited by low energy density. One of the reasons is that they are limited by narrow voltage window in aqueous-solution-based gel electrolytes [17]. Design the 3.0 V flexible supercapacitor for AC line filtering based on an ionic-liquid-based polymer gel electrolyte and carbon nanotube electrode material become emerging. Such flexible supercapacitor can exhibit 20 times higher areal energy density than that of the previously demonstrated 1.0 V flexible supercapacitor. Kang et al. [17] designed a 3.0 V flexible supercapacitor with CNT electrode materials based on a ionic-liquid-based polymer gel electrolyte that could be used for AC line filtering (Fig. 7f–i). The as-resulted supercapacitor had an approximately 20 times higher capacitance than the previously developed 1.0 V supercapacitor (0.66 vs 0.03 μWh/cm^2). The frequency response of flexible supercapacitors based on CNTs was closely related to the thickness of electrode materials. The phase angle increased from 70.6° to 82.7°, with the thickness of the

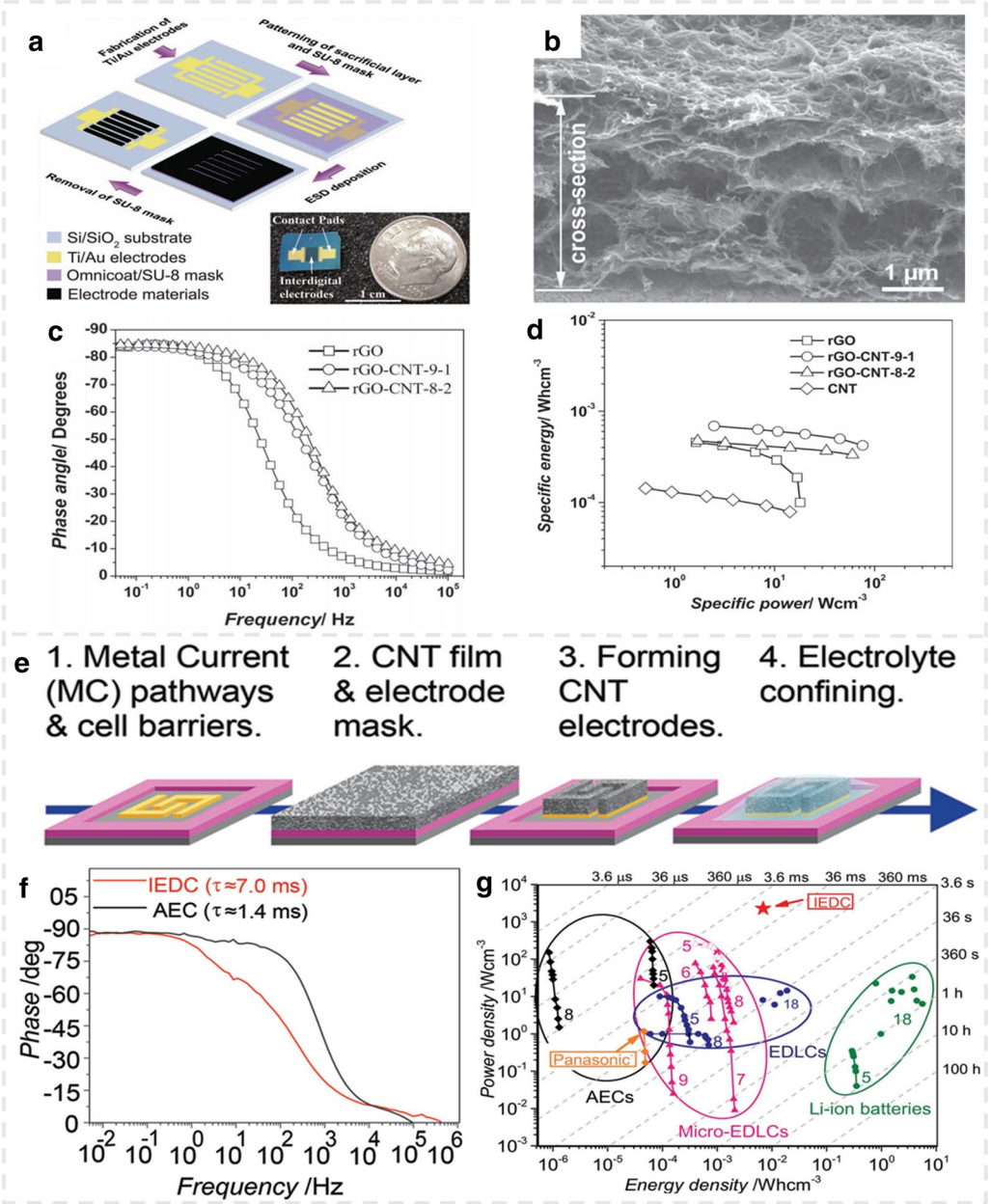

Fig. 6 **a** Schematic of the manufacturing process for rGO-CNT MSCs; **b** SEM of the deposited rGO-CNT composite; **c** phase angle versus the frequency for MSCs based on different rGO/CNT ratios; **d** Ragone plots showing the relationship of specific energy and power of MSCs; Reproduced with permission from Ref [50]. Copyright 2012. WILEY–VCH. **e** A simple fabrication process of integrated energy device circuits (IEDCs); **f** the dependence of the phase angle with frequency; and **g** Ragone plots of IEDCs compared with other energy storage devices. Reproduced with permission from Ref [48]. Copyright 2015. WILEY–VCH

film decreasing from 300 to 50 nm. The corresponding areal capacitance was reduced from 233 to 43 μF cm^{-2} at 120 Hz. Thus, the potential application of supercapacitors in flexible or portable electronic products was considerably improved by increasing the device voltage and simultaneously maintaining the rapid response ability.

In addition, most supercapacitors with AC line filtering performance take advantage of their high ionic conductivity in water, but limit the operating voltage to less than 1.0 V, and lead to the low power density of supercapacitors [17]. The basic requirement for expanding the voltage window is to design appropriate electrode

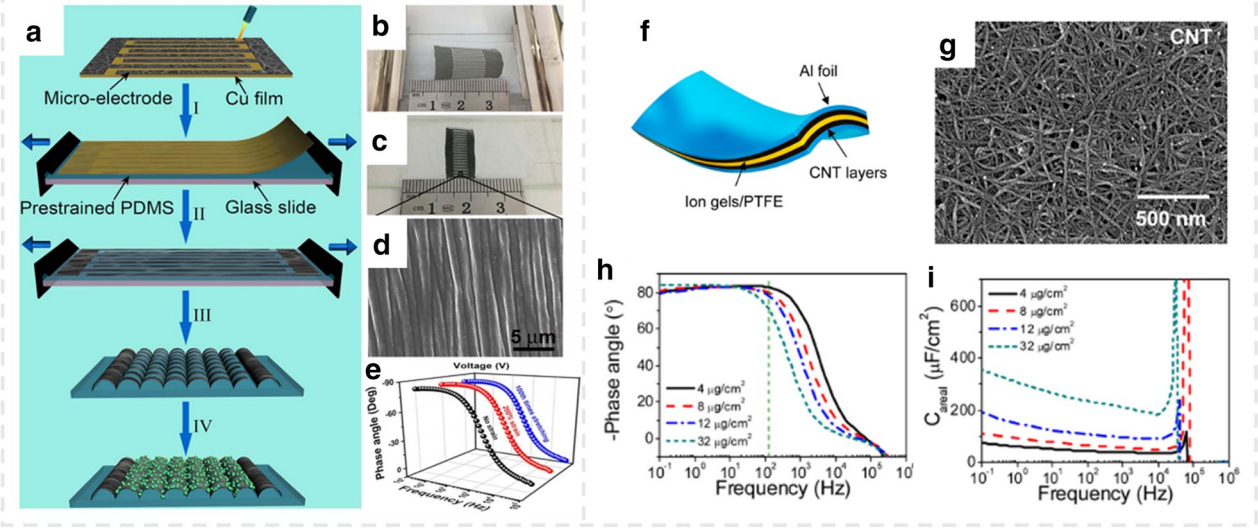

Fig. 7 **a** Schematic for the fabrication of stretchable MSCs; **b** optical image of the MSC under a strain force of 200%; **c** optical image of the MSC without any strain force; **d** SEM image of strain-free thin films; **e** phase angle versus the frequency under different strain forces; Reproduced with permission from Ref [72]. Copyright 2017. Elsevier. **f** Schematic of flexible all-solid-state supercapacitors; **g** SEM image of the CNT electrode; **h** dependence of the phase angle with frequency; and **i** dependence of frequency and areal capacitance. Reproduced with permission from Ref [17]. Copyright 2016. American Chemical Society

materials with a porous structure. Yoo [73] reported a supercapacitor with AC line filtering by using graphitic-OMC (GOMC or CMK-3) as the electrode material to increase the voltage window. The orderly network structure was formed by adding a small amount of CNTs into CMK-3 to meet the requirement of AC line-filtering performance. The CMK-3 particles with well-defined, wide-open pore structures are obtained by infiltrating and carbonizing the SBA-15 silica template (Fig. 8a). As can be seen from the TEM image in Fig. 8b, CMK-3 has a straight pore channel. Figure 8c and d show the frequency response of the CMK-3/CNT supercapacitor. The supercapacitor based on an organic electrolyte has an excellent frequency response and high area capacitance, and the phase angle could reach 80° at 120 Hz. The near-vertical Nyquist curve shows that the CMK-3/CNT supercapacitor had a lower equivalent series resistance (~0.25 Ω). Furthermore, the supercapacitor exhibited a high-area capacitance of 559 μF cm^{-2} at 120 Hz. Furthermore, the supercapacitor exhibited a very short relaxation time constant of 1 ms. The maximum areal capacitance reached up to 963 μF cm^{-2} at current density 1 mA cm^{-2} (Fig. 8e). The voltage value of CMK-3/CNT supercapacitors was 41 V compared with that of commercial AECs (Fig. 8f). The volume capacitance of the CMK-3/CNT supercapacitor at 2.5 V was 16.7 times of commercial AECs (50.2 mF cm^{-3} vs 3.0 mF cm^{-3}). Compared with the previously reported supercapacitors, the maximum voltages could reach only 3.4 V (VOGNs) [74] and 21 V (single walled nanotubes) [31]. The reason for the high voltage value of the CMK supercapacitor (41 V) compared with that of commercial AECs was the rationally designed electrode materials. The results showed that the high-frequency applications of supercapacitors could be developed through the optimization of the pore structure and increasing the conductivity of carbon electrode materials.

Other carbon-based electrodes

In addition to graphene and CNTs, other carbon-based electrode materials are used in the study of supercapacitors with AC line-filtering performance. The rapid frequency response is usually achieved by controlling the ordered pore structure of carbon materials. Kossyrev [75] examined carbon solutions for high-frequency–response applications of supercapacitors. The supercapacitors with carbon black as an electrode could meet the frequency response operation of AC line filtering because of the short length of the pore in the carbon black material. Furthermore, three samples S-1, S-2, and S-3 were prepared using different concentrations of the surfactant. The phase angle reached −75° at 120 Hz, and the RC time constant reached 0.354 ms. Medium/large pore camphore-derived carbon sponge-assembled button supercapacitors have been applied to AC line filtering with an ultrafast frequency response having a phase angle of 78° and a RC time constant of 319 ms at120 Hz [76]. Figure 9a shows the SEM images of carbon sponges

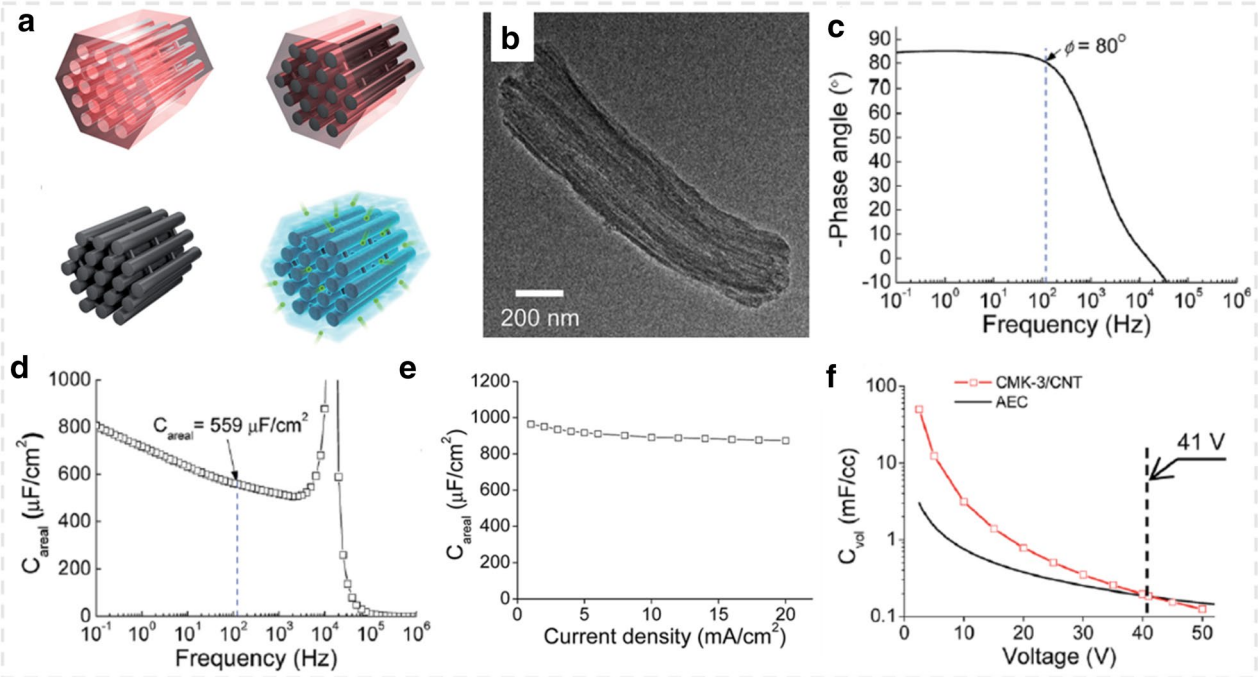

Fig. 8 **a** The flowchart of the preparation of graphitized CMK-3; **b** transmission electron microscopy (TEM) image of CMK-3; **c** dependent frequency and phase angle of the CMK-3 supercapacitor; **d** plot of the impedance phase angle versus the frequency; **e** areal capacitance with respect to current density; and **f** comparison of a CMK-3/CNT supercapacitor with a commercial AEC based on volumetric capacitance at different voltages. Reproduced with permission from Ref [73]. Copyright 2016. The Royal Society of Chemistry

of lyophilized S-3 that exhibited larger pores and a high degree of meso/macroporosity with sodium dodecyl sulfate (SDS) surfactant concentrations at 1 wt %. Figure 9b compares the frequency and phase angle of S-3, active carbon-based supercapacitor, and AEC. The phase angle of the S-3 carbon sponge (−78°) was considerably larger than that of the activated carbon-based capacitance (0°), which was comparable with that of the AEC (−85.5°). The capacitance was 172 mF cm^{-2}, and the RC time constant was 319 ms at 120 Hz (Fig. 9c, d).

Conducting polymer-based electrodes

In addition to the development of EDLCs with carbon-based electrodes for AC line filtering, various interesting conductive electrode material-based supercapacitors with AC line filtering have been reported. The electrochemical conductivity and high capacitance inherent of conductive polymer bridged the performance gap of the low-energy–density double-layered capacitors with carbon-based electrodes. Alshareef and coworkers [77] reported a polymer-based MSC with AC line-filtering performance other than a carbon-based electrochemical double-layer capacitor. Figure 10a shows the electropolymerization process for the preparation of a porous conductive polymer (PEDOT) electrode with an anionic surfactant at a lower anode potential. Figure 10b shows the nanomorphology of PEDOT with an open porous structure during electrochemical deposition. At 120 Hz (Fig. 10c), the impedance phase angle was 65° for the PEDOT-MSC. The PEDOT-MSCs exhibited a maximum areal capacitance of 9 mF cm^{-2} in 1 M H_2SO_4 and a volumetric stack capacitance of 50 F cm^{-3} (Fig. 10d). The Ragone plot (Fig. 10e) shows that the maximum energy density and power density of PEDOT-MSC based on the ionic gel were 7.7 mWh cm^{-3} and 850 mW cm^{-3}, respectively. Moreover, this energy density was significantly higher than that of carbon-based materials (E = 0.15–6 mWh cm^{-3}). Furthermore, Shi and coworkers [78] reported an EC-based on highly conductive H_2SO_4-treated PEDOT:PSS porous electrodes with a flexible graphite foil as a current collector (denoted as AT-PEDOT:PSS) with AC line-filtering performance. Figure 10f shows that the manufacturing process of AT-PEDOT:PSS on the graphite foil [78]. The PEDOT was doubled on cellulose, and the PEDOT:PSS solution penetrated paper fibers through the inherent microporous structure of the cellulose paper. All cellulose fiber frameworks were completely dissolved in H_2SO_4 solution, and moreover, the residual AT-PEDOT:PSS membrane inherited its porous structure. The AT-PEDOT:PSS SEM

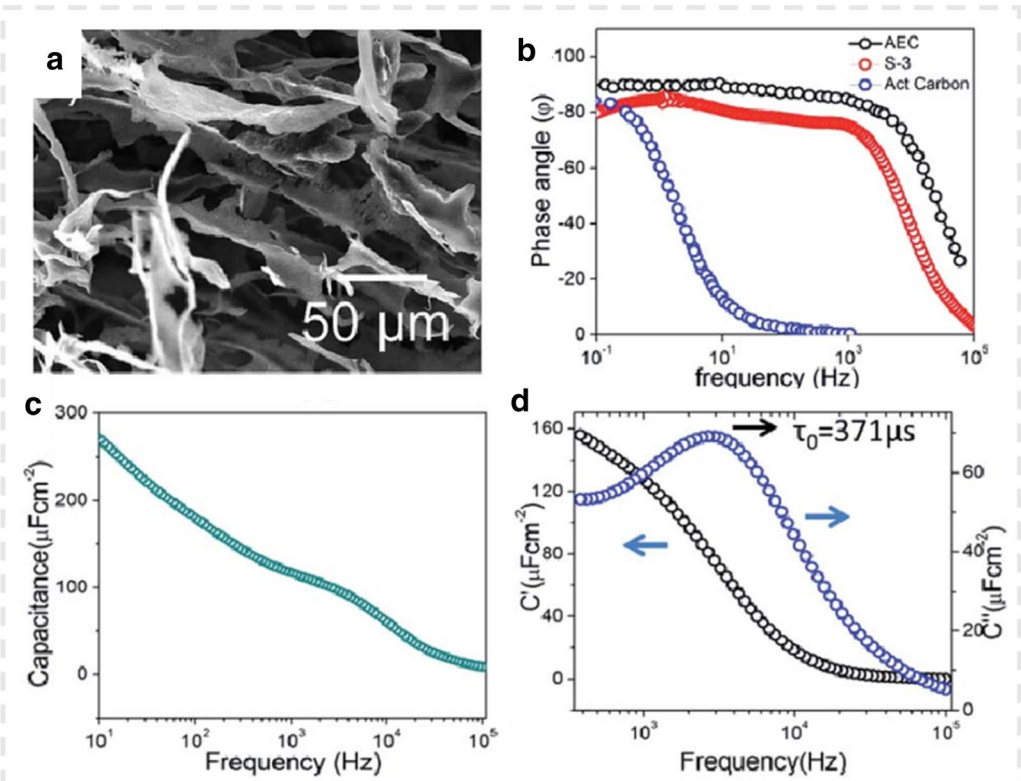

Fig. 9 **a** SEM image of carbon sponges with 1% SDS surfactant; **b** comparison of the frequency response of an S-3-based supercapacitor with that of the AEC and activated carbon-based supercapacitors; **c** frequency-dependent specific capacitance; and **d** real and imaginary parts of the capacitance of the S-3-based supercapacitor. Reproduced with permission from Ref [75]. Copyright 2015. The Royal Society of Chemistry

image showed that the micropore wall comprises nanoporous polymer nanoparticles (Fig. 10g). These material-based electrodes exhibited an excellent phase angle of 83.6° at 120 Hz with a short RC time constant of 0.15 ms (Fig. 10h). Concurrently, the ECs exhibited high areal capacitance (994 μF cm^{-2}), which was the highest value among the reported ECs with a phase angle of higher than 80° at 120 Hz [12, 60, 74]. It provides the possibility of replacing AECs, thereby reducing the size of electronic devices in future.

This study [19] reported a layer-by-layer (LBL) method for preparing on-chip MSCs with AC line-filtering performance by increasing an azulene-bridged coordination polymer framework (PiCBA) on the inter-digital Au electrode surface. Figure 11a–c show the procedure. The TEM image indicated a uniform macroscopic lateral dimension of the obtained coordination polymer film (Fig. 11d). An impedance phase angle of −73° was achieved at a frequency of 120 Hz (Fig. 11e). τ_{RC} obtained by calculating the Nyquist plot with imaginary capacitance was as short as 0.83 ms (Fig. 11f), thus indicating superior AC line-filtering performance. Highlighting the overall performance of the MSCs, the Ragone diagram for PiCBA-based MSCs exhibited a high energy and power density of 4.7 mWh cm^{-3} and 1323 W cm^{-3}, respectively (Fig. 11g). This study provided a potential solution for the fabrication of coordination polymer framework-based MSCs with AC line-filtering performance.

Supercapacitors have high capacitive properties; however, complex dynamics limit their frequency response in AC voltage. Park and coworkers [79] demonstrated porous MXene/conducting polymer hybrid-based ECs with AC line-filtering performance. Active materials were deposited through the spray-coating method, including $Ti_3C_2T_x$ MXene (denoted as Ti_3C_2) and Ti_3C_2/PEDOT:PSS hybrids, at a mass ratio of 1:1 and 1:2 (denoted as MP11 and MP12), respectively. Figure 12a shows the scalability of the spray-coating method for the ECs prepared with poly(vinyl alcohol)-hydroxyethyl methacrylate (PVA-HEMA) hydrogel. The SEM image of the hybrid thin film shows that the open mesoporous is essential to reduce pore tortuosity and ensure rapid charge transport. Figures 12c and d illustrate the Bode and frequency-dependent capacitance to verify the frequency response of Ti_3C_2, MP11, and MP12 to AC line filtering. The phase angles and RC time constants of Ti_3C_2,

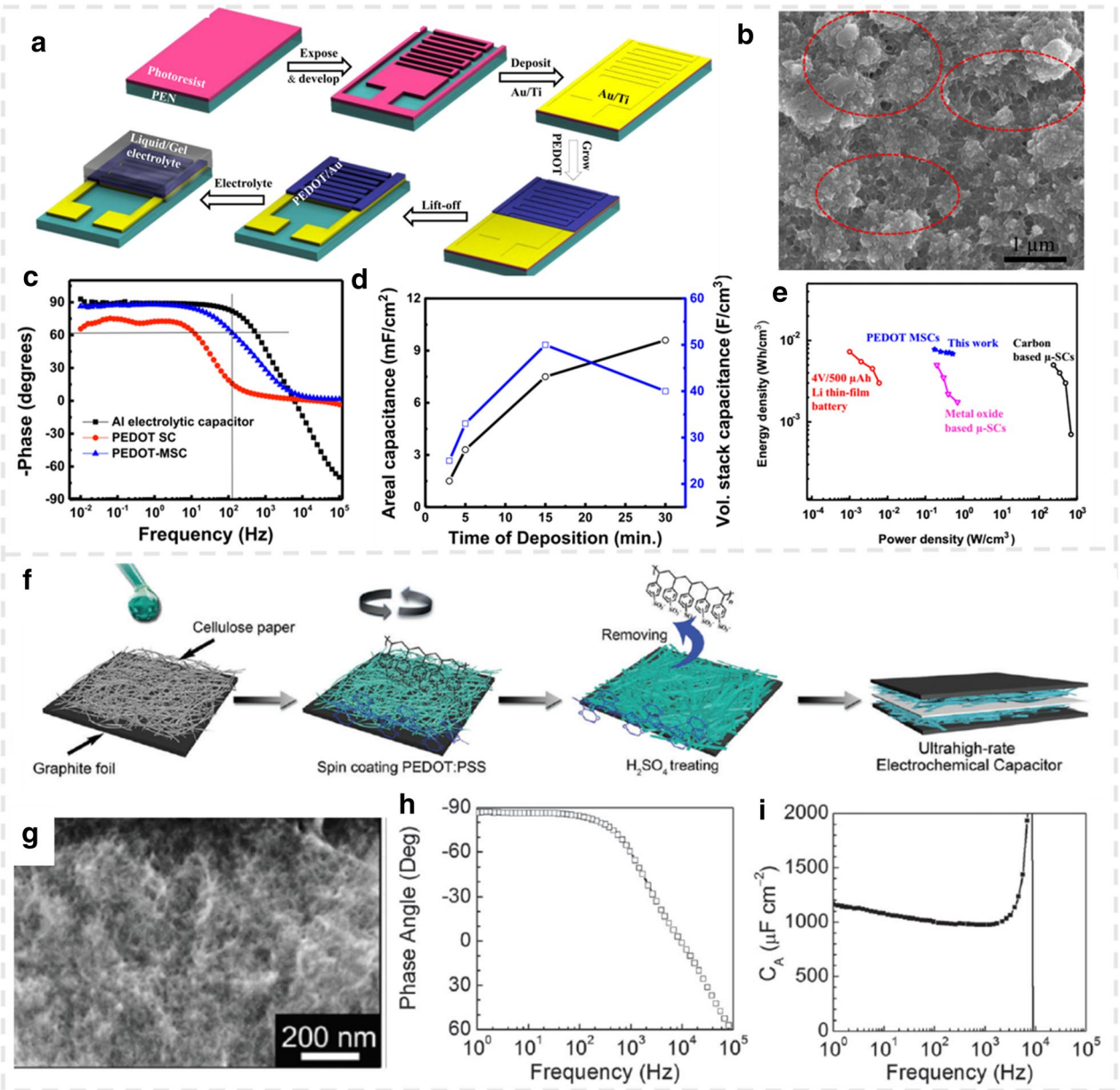

Fig. 10 **a** Schematic for the fabrication of PEDOT-MSCs; **b** SEM image of the as-prepared PEDOT thin film; **c** phase angle versus the frequency of the PEDOT-MSCs compared with a commercial AEC and conventional PEDOT supercapacitor; **d** areal and volumetric capacitance of PEDOT-MSCs at a current density of 35 μA cm^{-2}; **e** Ragone plots of Li thin-film batteries; carbon- and metal oxide-based MSCs, and PEDOT-MSC; Reproduced with permission from Ref [77]. Copyright 2015. Elsevier. **f** Schematic of the fabrication of AT-PEDOT:PSS; **g** SEM images of an AT-PEDOT:PSS/graphite foil composite; **h** frequency-dependent phase angle curve of a AT-PEDOT:PSS-based supercapacitor; and **i** plot of specific areal capacitance as a function of frequency. Reproduced with permission from Ref [78]. Copyright 2016. The Royal Society of Chemistry

MP11, and MP12 were 70.0°, 76.1°, and 79.1° at 120 Hz and 0.39, 0.12, and 0.29 ms, respectively (Fig. 12c). The areal/volumetric capacitances of Ti_3C_2, MP11, and MP12 ECs at 120 Hz were 0.006 mF cm^{-2}/0.24 F cm^{-3}, 0.302 mF cm^{-2}/8.51 F cm^{-3}, and 0.560 mF cm^{-2}/24.2 F cm^{-3}, respectively (Fig. 12d). The input AC signal was rectified into the pulse signal and was then smoothed through series MP12 ECs, and the output constant DC voltage was 1.27 V (Fig. 12e). The performance gap between high capacitance and the high frequency response was eliminated in this work, and the form-factor-free miniature and scalable devices could be realized. These results

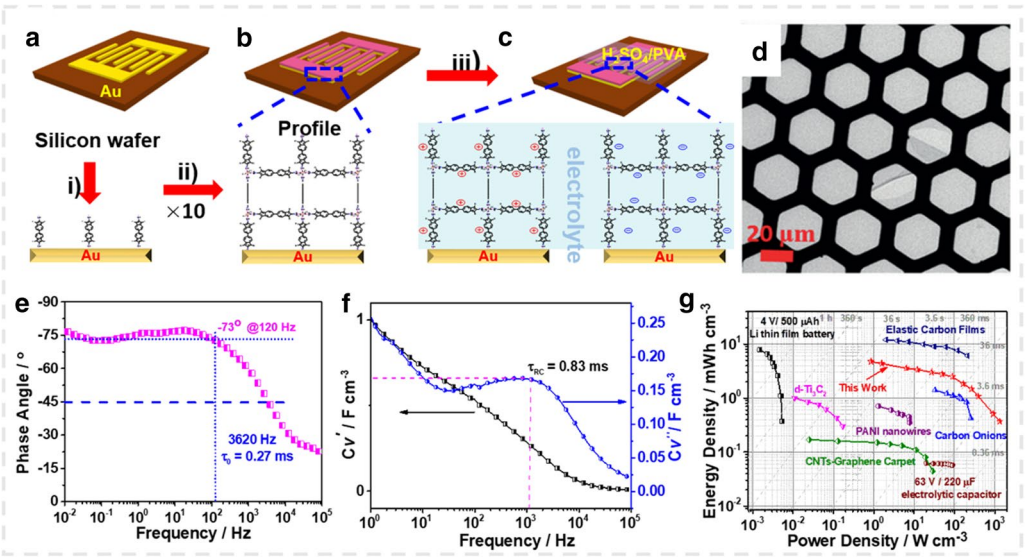

Fig. 11 **a**–**c** Schematic of LBL fabrication of a PiCBA film on Au interdigital electrodes; **d** TEM image shows a large area of a PiCBA film on a copper grid; **e** impedance phase angle on the frequency for the PiCBA-based MSC; **f** plot of capacitance versus the frequency of PiCBA-based MSCs; and **g** Ragone plots compared the energy and power density for PiCBA and reported supercapacitor and batteries. Reproduced with permission from Ref [19]. Copyright 2017. Wiley–VCH

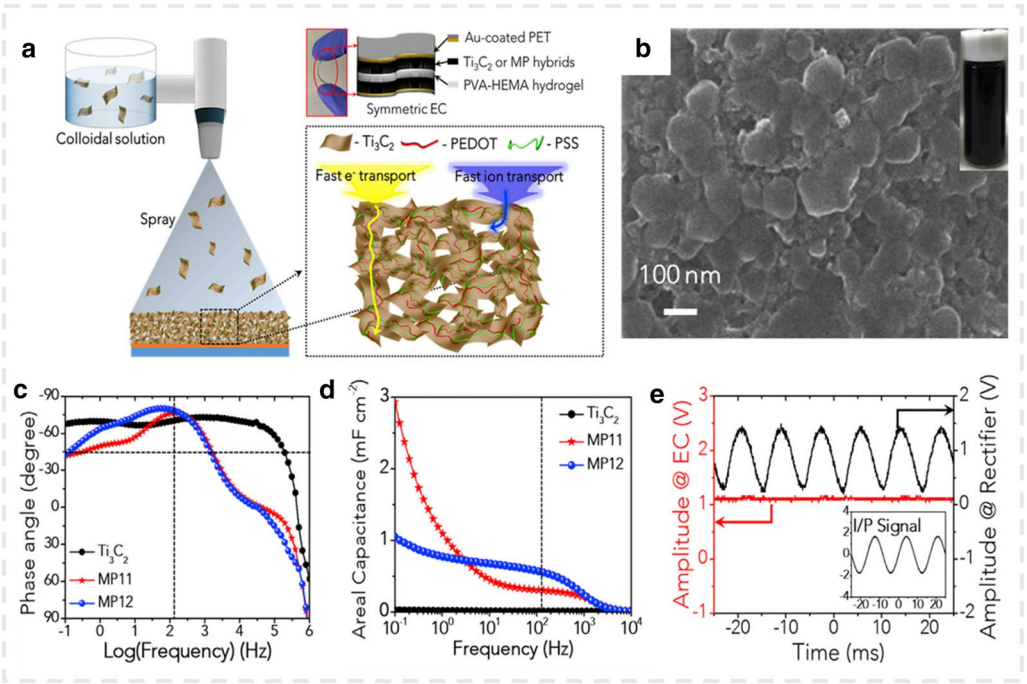

Fig. 12 **a** Schematic of the fabrication of a flexible Ti_3C_2/PEDOT:PSS hybrid electrode based on the spray-coating method; **b** SEM image of Ti_3C_2/PEDOT:PSS at a mass ratios of 1:2 thin film; **c** frequency-dependent phase angle, and **d** frequency-dependent areal capacitances of Ti_3C_2, MP11, and MP12 ECs; and **e** pulsating output signals across the rectifier and constant DC output across MP12 ECs at 60 Hz (Inset indicates AC input signal). Reproduced with permission from Ref [79]. Copyright 2019. Elsevier

emphasize the outstanding filtering performance of series MP12 ECs, which could be next-generation capacitors to replace AEC for AC line filtering.

Transition metal-based electrodes

Some interesting electrode materials combine a double-layer capacitor and pseudocapacitance effects and can be applied to the supercapacitor with AC line-filtering performance. For example, oxides, nitrides, and chalcogenides of transition metals have been widely investigated because of their additional pseudocapacitance contribution. Pseudo-capacitors can provide higher energy density through rapid redox reaction because of their charge transfer, but the limited electronic conductivity of most pseudo-capacitive oxides leads to high electrode resistance. Therefore, compared with electric double layer capacitors and electrolyte capacitors, pseudo-capacitors have lower power density [82]. To compensate for the low conductivity of electrode materials, pseudocapacitance materials are frequently used to bridge highly conductive graphene and similar carbon-based scaffolds.

Transition metal oxides are widely used in the development of high-energy–density supercapacitors because of the inherent large pseudocapacitance effect. However, a typical transition metal with high resistance would affect the charging and discharging rates of supercapacitors, thereby making their application for AC line filtering difficult. To overcome the challenge of low conductivity, a graphene-bridged V_2O_3/VO_x core–shell nanostructure electrode was reported [80]. The quasi-metallic V_2O_3 nanocores were dispersed on the conductive graphene sheet, and V_2O_3 was naturally formed with VO_2 and V_2O_5 as active materials. The interconnected graphene and V_2O_3 formed an electron conduction path, whereas the amorphous VOx shell promoted ion insertion/extraction to achieve high rate performance (Fig. 13a). SEM images of the synthesized rice-shaped vanadium oxide nanoparticles showed that the average diameter of the nanoparticles was 40 nm, and the covered rGO sheets were uniformly monolayer without clustering (Fig. 13b). Furthermore, H_2 heat treatment of the electrode material significantly improved conductivity. Such an EC with a charge–discharge rate of up to 50 V s^{-1} provided a power density of 1000 kW kg^{-1} at an energy density of 10 Wh kg^{-1}. The characteristic frequency was measured as 114 Hz at a phase angle of 45° (Fig. 13c, d). These observations indicated that graphene-composited transition metal oxides could be favorable for rapid EC development.

In recent years, metal nitrides as electrode materials for high-performance supercapacitors have received considerable attention because of their excellent conductivity [81]. Among them, the conductivity of titanium nitride (TiN) is between 4×10^3 and 5.55×10^4 S cm^{-1}, which is

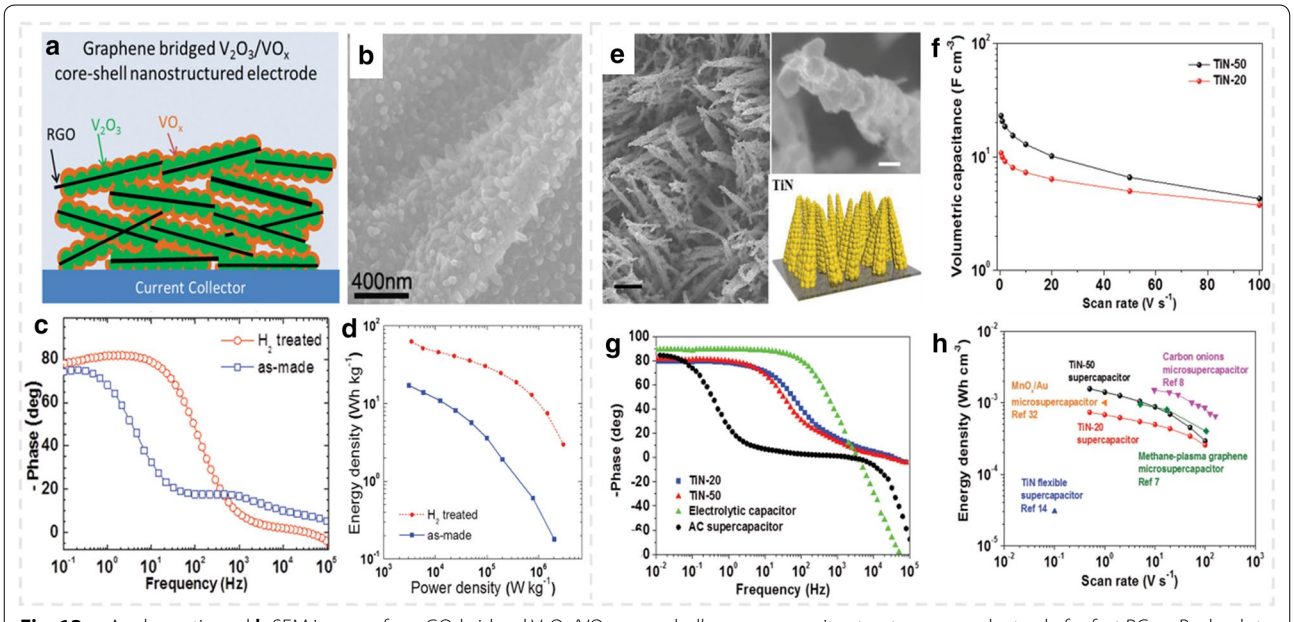

Fig. 13 **a** A schematic and **b** SEM image of an rGO-bridged V_2O_3/VOx core–shell nanocomposite structure as an electrode for fast PCs; **c** Bode plots and **d** Ragone plots of supercapacitors fabricated from hydrogen-treated and as-made nanocomposite; Reproduced with permission from Ref 80. Copyright 2014. WILEY–VCH. **e** cross-sectional SEM image of TiN-50 (scale bar: black 1 μm and white 100 nm); **f** volumetric capacitance versus the scan rate at 20 and 50 nm; **g** frequency-dependent phase angle for TiN-20, TiN-50, AECs, and an active carbon supercapacitor; and **h** volumetric energy density as a function of the scan rate. Reproduced with permission from Ref [81]. Copyright 2016. WILEY–VCH

close to that of metal and should improve the rate performance by providing rapid charge transport. Corn-like TiN nanostructures (Fig. 13e) exhibited capacitive performance at scan rates as high as 100 V s^{-1} in ultrafast-charging energy storage devices. Figure 13f, h compare the volumetric capacitance and energy density. A volumetric capacitance of 20.7 F cm^{-3} could be achieved. τ_0 values were approximately 4–2 ms (the corresponding characteristic frequencies were 40 and 80 Hz, respectively), which were considerably faster than 400 ms for the AC supercapacitor and was comparable to 0.3 ms for the electrolytic capacitor (Fig. 13g). At a scan rate of 1 V s^{-1}, TiN-50 and TiN-20 exhibit a volumetric capacitance of 20.7 and 10.0 F cm^{-3}, respectively, higher than that of active carbon (AC; 9.0 F cm^{-3}) and onion-like carbon (1.3 F cm^{-3}) under the same measurement condition [42, 44]. All these results conspicuously suggest that TiN has great potential for ultrahigh power and energy. Moreover, transition metal sulfides belong to the category of pseudocapacitance electrode materials. WS_2-, MoS_2-, and VS_2-based electrodes have been reported mainly because of their relatively large surface area and pseudocapacitance [82, 83]. However, these materials have no frequency response. Such materials can be further explored for AC line filtering.

AC line-filtering performance design

The design of supercapacitors with AC line-filtering performance depends on various influencing factors, including preparation of electrode materials, selection of electrolytes, method of preparing electrode materials, and assembly of the device. (1) The first concern is the preparation of electrode materials. Conventional supercapacitors with carbon-based materials exhibit a slow frequency response at 120 Hz because the complex pore structure restricts the transfer of charge [9]. Study and design of electrode materials with an adjustable pore structure or ordered pore structure for supercapacitors with AC line-filtering performance is necessary. Carbon materials have been developed as electrodes for most supercapacitors with AC line filtering, including VOGNs [12, 27, 60, 83], ErGOs [9], and CNTs [30, 48, 74], [9], graphene-PEDOT:PSS [26], and conducting polymers [19, 78–80]. The excellent frequency response of these carbon materials is primarily because of suitable conductivity and the open porous structure for the rapid transportation of electrolyte ions. Therefore, the rational designing and fabrication of highly conductive electrodes with optimized porous nanostructures can improve the performance of supercapacitors with AC line filtering. (2) The second concern is the selection of electrolytes. Aqueous electrolytes, organic electrolytes, and ionic liquids are the three primary types of electrolytes commonly used in supercapacitors. Among them, the aqueous electrolyte shows a rapid frequency response because of its high ionic conductivity; however, the voltage window is limited to 1 V, thus rendering the low energy density of supercapacitors. Ultrafast organic ECs [38] have organic electrolytes, such as the acetonitrile (AN) solution of tetraethylammonium-tetrafluoroborate. The voltage window can be extended to approximately 3 V, thus providing an energy density of 472 μF V^2 cm^{-2}, and the phase angle is −80.5° at 120 Hz. Kim's group [17] developed a 3-V flexible supercapacitor for AC line filtering by using an ionic-liquid-based polymer as a gel electrolyte. The supercapacitor exhibited 20 times higher areal energy density than the 1-V flexible supercapacitor (0.66 vs 0.03 μWh/cm^2). The expansion of the voltage window while maintaining the fast frequency response capability considerably increases the potential for the high-frequency application of supercapacitors in electronic devices. (3) The third concern is the rational preparation of electrode materials. So far, well-established synthetic methods, including electrochemical reduction, CVD, wet chemical synthesis, vacuum filtration, interfacial polymerization, laser scribing, inkjet printing, and screen printing, have been used for the preparation of electrode materials for supercapacitors with AC line-filtering performance [9, 19, 22, 26, 76, 84, 85]. The electrode materials prepared through different synthetic methods could have different structural characteristics, thus resulting in rapid mass transportation and excellent electrochemical properties. However, developing the structure–property relationship between synthetic methods, porous structures, specific capacitance, and AC line-filtering performance is difficult. (4) Finally, the configuration of the device is a concern. The structure and morphology of the electrode material can be controlled to ensure that the electrolyte permeates completely, and thus, the supercapacitor has AC filtering performance [87]. In view of the emergence of different electrode materials, the development of supercapacitors with excellent electrochemical properties provides a new possibility for energy storage. Conventionally, conventional supercapacitors have the sandwich-type structure [11]. In this case, the electrolyte is generally restricted from completely penetrating the electrode material, thus reducing the complete utilization of the electrochemical surface area of electrode materials. It is rarely expected to replace AECs with a large volume in electronic circuits for AC line filtering. An "in-plane" fabrication approach for ultrathin supercapacitors can guarantee each electrode with an effective mass (ions) contact without using a separator. Such a planar structure established a solid foundation for the further development of interdigital electrode MSCs. So far, several well-established synthetic methods have been used

Table 1 Representative results of supercapacitors with AC line-filtering performance

Electrode materials	Electrolyte	Phase angle at 120 Hz	f (kHz) at − 45°	τ_0 (ms)	τ_{RC} at 120 Hz	Specific capacitance	References
VOG	KOH	85	20	0.05	–	265 μFcm^{-2}	[60]
VOG	KOH	~ 90		32.8	–	30 F g^{-1}	[81]
ErGO	KOH	84	4.2	0.17	1.35	283 μFcm^{-2}	[9]
GO film	H_2SO_4			13.3		125 F g^{-1}	[85]
EOG	KOH	82	4.03		0.205	0.72 mFcm^{-2}	[86]
EOG	KOH	83	12		0.110	0.6 mFcm^{-2}	[88]
NHG	KOH	81.2	1.2		0.203	0.956 mFcm^{-2}	[89]
GO@CNT	NaSO4	81.5		0.82	0.19	662 μFcm^{-2}	[14]
CNT	H_2SO_4	81	1.425	0.701	0.199	1.202 mFcm^{-2}	[30]
SWCNT	TEABF4	82.2	1.995		0.501	0.564 mFcm^{-2}	[71]
GOMC/CNT	TEABF4	80.0	1.0	1.0		0.56 mFcm^{-2}	[70]
Carbon sponges	KOH	78		0.37	0.32	172 mFcm^{-2}	[73]
PENOT:PSS	H_2SO_4	84		0.59	0.15	994 mFcm^{-2}	[75]
PiCBA	H_2SO_4/PVA	73	3.62	0.27	0.83	34.1 Fcm^{-3}	[19]
Ti3C2/PEDOT:PSS	H_2SO_4/PHEMA/PVA	79.1	1.41	0.709	0.29	0.56 mFcm^{-2}	[76]

to prepare in-plane MSCs, such as laser scribing, inkjet printing, and photolithography. Many in-plane MSCs exhibit a superior frequency response, which allows their application in next-generation electronic devices for AC line filtering.

The design of supercapacitors with AC filtering performance could be affected by the above mentioned or other factors, e.g., the electrode material with high conductivity, controllable pore size matched the sizes of electrolyte ions, the distance between the electrodes is short enough to promote the rapid transportation of electrolyte ions. Therefore, micro-sized supercapacitor has sufficient advantages in the synthesis of capacitors with AC filtering properties. To provide an improved overview of this field, Table 1 presents the recent progress in AC line-filtering supercapacitors.

Conclusion

In this review, we summarized the research works in the field of supercapacitors with AC filtering performance. The applications of different electrode materials in the preparation of supercapacitors with AC line filtering are discussed. At the same time, some primary factors which could affect the AC filtering performance have been discussed. Compared with the traditional carbon-based electrode materials, the design of electrode materials with high electronic conductivity and using selected electrolytes with suitable aperture, the micro-supercapacitors with short electrode distance are more suitable for the development of capacitors with AC filtering performance.

Because in 2010, Miller first reported the new application of vertically oriented graphene-based supercapacitors in AC filtering, the interesting field has received considerable attention from various researchers and made unexpected remarkable progress. In addition to graphene-based electrode materials, several other electrode materials, including carbon-based materials (CNT, OLC, carbon sponges) and noncarbon-based materials (conducting polymer and transition metal), have been used in the research of AC line filtering and made outstanding achievement. On the basis of the research and discussion of designing supercapacitors with excellent overfiltering performance in the previous study, developing AC line filtering by synthesizing highly conductive electrode materials with an ordered pore structure and selecting an appropriate preparation process and electrolyte for device assembly would be ideal. Although a large number of supercapacitors have been reported and applied to AC line filtering, more efforts are required to apply them to practical electronic circuits, thus encouraging researchers to further develop supercapacitors for AC line filtering and other potential applications.

Abbreviations

AC: alternating current; DC: direct current; AECs: aluminum electrolytic capacitors; EDLCs: electrical double-layer capacitors; PCs: pseudocapacitors; EC: electrochemical capacitors; VOGN: oriented graphene nanosheet; CVD: chemical vapor deposition; ErGOs: electrochemically reduced graphene oxides; OMC: ordered mesoporous carbon; DLCs: double-layer capacitors; RC: resistance capacitance; CNT: carbon nanotube; MSCs: micro-supercapacitors; FS: femto-laser; NCNT: nitrogen-doped carbon nanotube; AFM: atomic-force microscopy; MG-MSCs: graphene-based micro-supercapacitors; SDS: sodium dodecyl sulfate; PEDOT: porous conductive polymer; PiCBA: azulene-bridged coordination polymer framework; TiN: titanium nitride.

Acknowledgements
Not available.

Authors' contributions
XZ, SH and EK conceived the content of the article and revised the text. DZ collected the literature, DZ, KJ, JL, XZ, CK co-wrote and revised the paper. All authors read and approved the final manuscript.

Funding
This work was financially supported by National Key Research and Development Program of China (2017YFE9134000), Greece-China joint R&D project Calypso (T7ΔΚΙ-00039), co-financed by Greece, the EU Regional Development Fund and the Chinese Ministry of Science and Technology, NSFC Excellent Young Scientists Fund (51722304), NSFC (51973114, 21720102002, 51811530013, 21406220, 21878188), Shanghai Pujiang Talent Program (18PJ1406100).

Availability of data and materials
Not applicable.

Competing interests
X. Zhuang and E. Kymakis are the Editorial Board Member and Section Editor of BMC Materials, respectively. The authors declare that the draft has gone through official peer review procedure before publication.

Author details
[1] The Meso-Entropy Matter Lab, School of Chemistry and Chemical Engineering, Shanghai Key Laboratory of Electrical Insulation and Thermal Aging, State Key Laboratory of Metal Matrix Composites, Shanghai Jiao Tong University, Dongchuan Road 800, Shanghai 200240, China. [2] School of Chemical and Environmental Engineering, Shanghai Institute of Technology, Haiquan Road 100, Shanghai 201418, China. [3] School of Information and Communication Technology, KTH Royal Institute of Technology, Electrum 229, 16440 Kista, Sweden. [4] State Key Laboratory for Oxo Synthesis and Selective Oxidation, Suzhou Research Institute of Lanzhou Institute of Chemical Physics, Chinese Academy of Sciences, Suzhou 215000, China. [5] School of Mechanical Engineering, Shanghai Jiao Tong University, Shanghai 200240, China. [6] Department of Electrical and Computer Engineering, Hellenic Mediterranean University, Estavromenos, 71410 Heraklion, Crete, Greece. [7] Jiangsu Key Laboratory of Environmentally Friendly Polymeric Materials, School of Materials Science and Engineering, Changzhou University, Changzhou 213164, China.

Received: 25 July 2019 Accepted: 12 January 2020
Published online: 05 February 2020

References

1. Doval-Gandoy J, Castro C, Martinez MC. Line input AC-to-DC conversion and filter capacitor design. IEEE Trans Ind Appl. 2003;39:1169–76.
2. Chang Y-H, Lin Y-K. Design and analysis of high-gain switched-capacitor-inductor-based inverter for step-up DC-AC conversion. J Circuit Syst Comput. 2018;27:1850030.
3. Miller JR. Graphene double-layer capacitor with ac line-filtering performance. Science. 2010;329:1637–9.
4. Sheng K, Sun Y, Li C, Yuan W, Shi G. Ultrahigh-rate supercapacitors based on eletrochemically reduced graphene oxide for ac line-filtering. Sci Rep. 2012;2:247.
5. Augustyn V, Simon P, Dunn B. Pseudocapacitive oxide materials for high-rate electrochemical energy storage. Energy Environ Sci. 2014;7:1597–614.
6. Bonaccorso F, Colombo L, Yu G, Stoller M, Tozzini V, Ferrari AC, et al. Graphene, related two-dimensional crystals, and hybrid systems for energy conversion and storage. Science. 2015;347:1246501.
7. Lukatskaya MR, Dunn B, Gogotsi Y. Multidimensional materials and device architectures for future hybrid energy storage. Nat Commun. 2016;7:12647.
8. Wang Y, Song Y, Xia Y. Electrochemical capacitors: mechanism, materials, systems, characterization and applications. Chem Soc Rev. 2016;45:5925–50.
9. Chao D, Liang P, Chen Z, Bai L, Shen H, Liu X, et al. Pseudocapacitive Na-Ion storage boosts high rate and areal capacity of self-branched 2D layered metal chalcogenide nanoarrays. ACS Nano. 2016;10:10211–9.
10. Chao D, Zhu C, Yang P, Xia X, Liu J, Wang J, et al. Array of nanosheets render ultrafast and high-capacity Na-ion storage by tunable pseudocapacitance. Nat Commun. 2016;7:12122.
11. Honda Y, Haramoto T, Takeshige M, Shiozaki H, Kitamura T, Ishikawa M. Aligned MWCNT sheet electrodes prepared by transfer methodology providing high-power capacitor performance. Electrochem Solid ST. 2007;10:A106–10.
12. Toupin M, Bélanger D, Hill IR, Quinn D. Performance of experimental carbon blacks in aqueous supercapacitors. J Power Sour. 2005;140:203–10.
13. Wang F, Wu X, Yuan X, Liu Z, Zhang Y, Fu L, et al. Latest advances in supercapacitors: from new electrode materials to novel device designs. Chem Soc Rev. 2017;46:6816–54.
14. Cai M, Outlaw RA, Butler SM, Miller JR. A high density of vertically-oriented graphenes for use in electric double layer capacitors. Carbon. 2012;50:5481–8.
15. Lin J, Zhang C, Yan Z, Zhu Y, Peng Z, Hauge RH, et al. 3-Dimensional graphene carbon nanotube carpet-based microsupercapacitors with high electrochemical performance. Nano Lett. 2013;13:72–8.
16. Kang YJ, Yoo Y, Kim W. 3-V solid-state flexible supercapacitors with ionic-liquid-based polymer gel electrolyte for AC line filtering. ACS Appl Mater Interface. 2016;8:13909–17.
17. Eftekhari A, Fan Z. Ordered mesoporous carbon and its applications for electrochemical energy storage and conversion. Mater Chem Front. 2017;1:1001–27.
18. Yang C, Schellhammer KS, Ortmann F, Sun S, Dong R, Karakus M, et al. Coordination Polymer Framework Based On-Chip Micro-Supercapacitors with AC Line-Filtering Performance. Angew Chem Int Edit. 2017;56:3920–4.
19. Bo Z, Wen Z, Kim H, Lu G, Yu K, Chen J. One-step fabrication and capacitive behavior of electrochemical double layer capacitor electrodes using vertically-oriented graphene directly grown on metal. Carbon. 2012;50:4379–87.
20. Cao X, Shi Y, Shi W, Lu G, Huang X, Yan Q, et al. Preparation of novel 3D graphene networks for supercapacitor applications. Small. 2011;7:3163–8.
21. Gao W, Singh N, Song L, Liu Z, Reddy ALM, Ci L, et al. Direct laser writing of micro-supercapacitors on hydrated graphite oxide films. Nat Nanotechnol. 2011;6:496.
22. Huang H, Tang Y, Xu L, Tang S, Du Y. Direct formation of reduced graphene oxide and 3D lightweight nickel network composite foam by hydrohalic acids and its application for high-performance supercapacitors. ACS Appl Mater Interface. 2014;6:10248–57.
23. Premathilake D, Outlaw RA, Parler SG, Butler SM, Miller JR. Electric double layer capacitors for ac filtering made from vertically oriented graphene nanosheets on aluminum. Carbon. 2017;111:231–7.
24. Wu Z, Li L, Lin Z, Song B, Li Z, Moon K-S, et al. Alternating current line-filter based on electrochemical capacitor utilizing template-patterned graphene. Sci Rep. 2015;5:10983.
25. Wu ZS, Liu Z, Parvez K, Feng X, Mullen K. Ultrathin printable graphene supercapacitors with AC line-filtering performance. Adv Mater. 2015;27:3669–75.
26. Yoon Y, Lee K, Kwon S, Seo S, Yoo H, Kim S, et al. Vertical Alignments of graphene sheets spatially and densely piled for fast ion diffusion in compact supercapacitors. ACS Nano. 2014;8:4580–90.
27. Eftekhari A. The mechanism of ultrafast supercapacitors. J Mater Chem A. 2018;6:2866–76.
28. Li W, Islam N, Ren G, Li S, Fan Z. AC-filtering supercapacitors based on edge oriented vertical graphene and cross-linked carbon nanofiber. Materials. 2019;12:604.
29. Zhuang X, Mai Y, Wu D, Zhang F, Feng X. Two-dimensional soft nanomaterials: a fascinating world of materials. Adv Mater. 2015;27:403–27.
30. Rangom Y, Tang X, Nazar LF. Carbon nanotube-based supercapacitors with excellent ac line filtering and rate capability via improved interfacial impedance. ACS Nano. 2015;9:7248–55.
31. Zhu J, Yang C, Lu C, Zhang F, Yuan Z, Zhuang X. Two-dimensional porous polymers: from sandwich-like structure to layered skeleton. Acc Chem Res. 2018;51:3191–202.
32. Wei L, Jiang W, Yuan Y, Goh K, Yu D, Wang L, et al. Synthesis of free-standing carbon nanohybrid by directly growing carbon nanotubes on

air-sprayed graphene oxide paper and its application in supercapacitor. J Solid State Chem. 2015;224:45–51.
33. Krishnamoorthy K, Pazhamalai P, Sahoo S, Kim S-J. Titanium carbide sheet based high performance wire type solid state supercapacitors. J Mater Chem A. 2017;5:5726–36.
34. Shuai X, Bo Z, Kong J, Yan J, Cen K. Wettability of vertically-oriented graphenes with different intersheet distances. RSC Adv. 2017;7:2667–75.
35. Xie X, He X, Shao X, Dong S, Xiao N, Qiu J. Synthesis of layered microporous carbons from coal tar by directing, space-confinement and self-sacrificed template strategy for supercapacitors. Electrochim Acta. 2017;246:634–42.
36. Dokko K, Mohamedi M, Fujita Y, Itoh T, Nishizawa M, Umeda M, et al. Kinetic characterization of single particles of $LiCoO_2$ by AC impedance and potential step methods. J Electrochem Soc. 2001;148:A422–6.
37. Chi F, Li C, Zhou Q, Zhang M, Chen J, Yu X, et al. Graphene-based organic electrochemical capacitors for AC line filtering. Adv Energy Mater. 2017;7:1700591.
38. Kyerematen NA, Brousse T, Pech D. Microsupercapacitors as miniaturized energy-storage components for on-chip electronics. Nat Nanotechnol. 2016;12:7.
39. Zhang P, Wang F, Yu M, Zhuang X, Feng X. Two-dimensional materials for miniaturized energy storage devices: from individual devices to smart integrated systems. Chem Soc Rev. 2018;47:7426–51.
40. Zhang C, Lu C, Zhang F, Qiu F, Zhuang X, Feng X. Two-dimensional organic cathode materials for alkali-metal-ion batteries. J Energy Chem. 2018;27:86–98.
41. Pech D, Brunet M, Durou H, Huang P, Mochalin V, Gogotsi Y, et al. Ultrahigh-power micrometre-sized supercapacitors based on onion-like carbon. Nat Nanotechnol. 2010;5:651.
42. Fan Z, Islam N, Bayne SB. Towards kilohertz electrochemical capacitors for filtering and pulse energy harvesting. Nano Energy. 2017;39:306–20.
43. Zhu Y, Murali S, Stoller MD, Ganesh KJ, Cai W, Ferreira PJ, et al. Carbon-based supercapacitors produced by activation of graphene. Science. 2011;332:1537.
44. Gamby J, Taberna PL, Simon P, Fauvarque JF, Chesneau M. Studies and characterisations of various activated carbons used for carbon/carbon supercapacitors. J Power Sources. 2001;101:109–16.
45. An KH, Kim WS, Park YS, Moon J-M, Bae DJ, Lim SC, et al. Electrochemical properties of high-power supercapacitors using single-walled carbon nanotube electrodes. Adv Fun Mater. 2001;11:387–92.
46. Du C, Pan N. Supercapacitors using carbon nanotubes films by electrophoretic deposition. J Power Sources. 2006;160:1487–94.
47. Laszczyk KU, Kobashi K, Sakurai S, Sekiguchi A, Futaba DN, Yamada T, et al. Lithographically integrated microsupercapacitors for compact, high performance, and designable energy circuits. Adv Energy Mater. 2015;5:1500741.
48. Li X, Rong J, Wei B. Electrochemical behavior of single-walled carbon nanotube supercapacitors under compressive stress. ACS Nano. 2010;4:6039–49.
49. Majid B, Chunlei W. Micro-supercapacitors based on interdigital electrodes of reduced graphene oxide and carbon nanotube composites with ultrahigh power handling performance. Adv Fun Mater. 2012;22:4501–10.
50. Butler SZ, Hollen SM, Cao L, Cui Y, Gupta JA, Gutiérrez HR, et al. Progress, challenges, and opportunities in two-dimensional materials beyond graphene. ACS Nano. 2013;7:2898–926.
51. Zhao D, Chang W, Lu C, Yang C, Jiang K, Chang X, et al. Charge transfer salt and graphene heterostructure-based micro-supercapacitors with alternating current line-filtering performance. Small. 2019;0:1901494.
52. Xu M, Liang T, Shi M, Chen H. Graphene-like two-dimensional materials. Chem Rev. 2013;113:3766–98.
53. Zhao J, Zhang Y, Yan J, Zhao X, Xie J, Luo X, et al. Fiber-shaped electrochemical capacitors based on plasma-engraved graphene fibers with oxygen vacancies for alternating current line filtering performance. ACS Appl Energy Mater. 2019;2:993–9.
54. Hosono H. Recent progress in transparent oxide semiconductors: materials and device application. Thin Solid Films. 2007;515(15):6000–14.
55. Rogers J A. Materials and mechanics for stretchable electronics—from electronic eye cameras to conformal brain monitors. TRANSDUCERS 2009–2009 International Solid-State Sensors, Actuators and Microsystems Conference. 2009:1602–1603.
56. Meng Y, Zhao Y, Hu C, Cheng H, Hu Y, Zhang Z, et al. All-graphene core-sheath microfibers for all-solid-state, stretchable fibriform supercapacitors and wearable electronic textiles. Adv Mater. 2013;25:2326–31.
57. Chen T, Xue Y, Roy AK, Dai L. Transparent and stretchable high-performance supercapacitors based on wrinkled graphene electrodes. ACS Nano. 2014;8:1039–46.
58. Jost K, Dion G, Gogotsi Y. Textile energy storage in perspective. J Mater Chem A. 2014;2:10776–87.
59. Miller JR, Outlaw RA. Vertically-oriented graphene electric double layer capacitor designs. J Electrochem Soc. 2015;162(5):A5077–82.
60. Cai M, Outlaw RA, Quinlan RA, Premathilake D, Butler SM, Miller JR. Fast response, vertically oriented graphene nanosheet electric double layer capacitors synthesized from C2H2. ACS Nano. 2014;8:5873–82.
61. Yoo JJ, Balakrishnan K, Huang J, Meunier V, Sumpter BG, Srivastava A, et al. Ultrathin planar graphene supercapacitors. Nano Lett. 2011;11:1423–7.
62. El-Kady MF, Kaner RB. Scalable fabrication of high-power graphene micro-supercapacitors for flexible and on-chip energy storage. Nat Commun. 2013;4:1475.
63. Li RZ, Peng R, Kihm KD, Bai S, Bridges D, Tumuluri U, et al. High-rate in-plane micro-supercapacitors scribed onto photo paper using in situ femtolaser-reduced graphene oxide/Au nanoparticle microelectrodes. Energy Environ Sci. 2016;9:1458–67.
64. Lim J, Narayan Maiti U, Kim N-Y, Narayan R, Jun Lee W, Sung Choi D, et al. Dopant-specific unzipping of carbon nanotubes for intact crystalline graphene nanostructures. Nat Commun. 2016;7:10364.
65. Zhao L, He R, Rim KT, Schiros T, Kim KS, Zhou H, et al. Visualizing individual nitrogen dopants in monolayer graphene. Science. 2011;333:999–1003.
66. Mane GP, Talapaneni SN, Anand C, Varghese S, Iwai H, Ji Q, et al. Preparation of Highly Ordered Nitrogen-Containing Mesoporous Carbon from a Gelatin Biomolecule and its Excellent Sensing of Acetic Acid. Adv Funct Mater. 2012;22:3596–604.
67. Ye J, Tan H, Wu S, Ni K, Pan F, Liu J, et al. Direct laser writing of graphene made from chemical vapor deposition for flexible, integratable micro-supercapacitors with ultrahigh power output. Adv Mater. 2018;30:1801384.
68. Wu ZS, Tan YZ, Zheng S, Wang S, Parvez K, Qin J, et al. Bottom-up fabrication of sulfur-doped graphene films derived from sulfur-annulated nanographene for ultrahigh volumetric capacitance micro-supercapacitors. J Am Chem Soc. 2017;139:4506–12.
69. Wu ZS, Parvez K, Feng X, Müllen K. Graphene-based in-plane micro-supercapacitors with high power and energy densities. Nat Commun. 2013;4:2487.
70. Wang S, Wu ZS, Zheng S, Zhou F, Sun C, Cheng H-M, et al. Scalable fabrication of photochemically reduced graphene-based monolithic micro-supercapacitors with superior energy and power densities. ACS Nano. 2017;11:4283–91.
71. Chen C, Cao J, Wang X, Lu Q, Han M, Wang Q, et al. Highly stretchable integrated system for micro-supercapacitor with AC line filtering and UV detector. Nano Energy. 2017;42:187–94.
72. Yoo Y, Kim M-S, Kim J-K, Kim YS, Kim W. Fast-response supercapacitors with graphitic ordered mesoporous carbons and carbon nanotubes for AC line filtering. J Mater Chem A. 2016;4:5062–8.
73. Yoo Y, Kim S, Kim B, Kim W. 2.5 V compact supercapacitors based on ultrathin carbon nanotube films for AC line filtering. J Mater Chem A. 2015;3:11801–6.
74. Kossyrev P. Carbon black supercapacitors employing thin electrodes. J Power Sour. 2012;201:347–52.
75. Joseph J, Paravannoor A, Nair SV, Han ZJ, Ostrikov K, Balakrishnan A. Supercapacitors based on camphor-derived meso/macroporous carbon sponge electrodes with ultrafast frequency response for ac line-filtering. J Mater Chem A. 2015;3:14105–8.
76. Kurra N. Conducting polymer micro-supercapacitors for flexible energy storage and Ac line-filtering. Nano Energy. 2015;13:500–8.
77. Zhang M, Zhou Q, Chen J, Yu X, Huang L, Li Y, et al. An ultrahigh-rate electrochemical capacitor based on solution-processed highly conductive PEDOT:PSS films for AC line-filtering. Energy Environ Sci. 2016;9:2005–10.
78. Gund GS, Park JH, Harpalsinh R, Kota M, Shin JH, Kim T-I, et al. MXene/polymer hybrid materials for flexible AC-filtering electrochemical capacitors. Joule. 2019;3:164–76.
79. Pan X, Ren G, Hoque MNF, Bayne S, Zhu K, Fan Z. Fast supercapacitors based on graphene-bridged V_2O_3/VOx core-shell nanostructure

electrodes with a power density of 1 MW kg^{-1}. Adv Mater Interface. 2014;1:1400398.
80. Yang P, Chao D, Zhu C, Xia X, Zhang Y, Wang X, et al. Ultrafast-charging supercapacitors based on corn-like titanium nitride nanostructures. Adv Sci. 2016;3:1500299.
81. Feng J, Sun X, Wu C, Peng L, Lin C, Hu S, et al. Metallic few-layered VS2 ultrathin nanosheets: high two-dimensional conductivity for in-plane supercapacitors. J Am Chem Soc. 2011;133:17832–8.
82. Savjani N, Lewis EA, Bissett MA, Brent JR, Dryfe RAW, Haigh SJ, et al. Synthesis of lateral size-controlled monolayer 1H-MoS2@Oleylamine as supercapacitor electrodes. Chem Mater. 2016;28:657–64.
83. Bo Z, Zhu W, Ma W, Wen Z, Shuai X, Chen J, et al. Vertically oriented graphene bridging active-layer/current–collector interface for ultrahigh rate supercapacitors. Adv Mater. 2013;25:5799–806.
84. Li J, Sollami Delekta S, Zhang P, Yang S, Lohe MR, Zhuang X, et al. Scalable fabrication and integration of graphene microsupercapacitors through full inkjet printing. ACS Nano. 2017;11:8249–56.
85. Zhou F, Huang H, Xiao C, Zheng S, Shi X, Qin J, et al. Electrochemically scalable production of fluorine-modified graphene for flexible and high-energy ionogel-based microsupercapacitors. J Am Chem Soc. 2018;140:8198–205.
86. Yang X, Zhu J, Qiu L, Li D. Bioinspired effective prevention of restacking in multilayered graphene films: towards the next generation of high-performance supercapacitors. Adv Mater. 2011;23:2833–8.
87. Ren G, Pan X, Bayne S, Fan Z. Kilohertz ultrafast electrochemical supercapacitors based on perpendicularly-oriented graphene grown inside of nickel foam. Carbon. 2014;71:94–101.
88. Ren G, Li S, Fan Z-X, Hoque MNF, Fan Z. Ultrahigh-rate supercapacitors with large capacitance based on edge oriented graphene coated carbonized cellulous paper as flexible freestanding electrodes. J Power Sources. 2016;325:152–60.
89. Zhou Q, Zhang M, Chen J, Hong J-D, Shi G. Nitrogen-doped holey graphene film-based ultrafast electrochemical capacitors. ACS Appl Mater Interfaces. 2016;8:20741–7.

Publisher's Note